



Deposited via The University of Leeds.

White Rose Research Online URL for this paper:

<https://eprints.whiterose.ac.uk/id/eprint/136028/>

Version: Accepted Version

Article:

Malmierca-Vallet, I, Sime, LC, Tindall, JC et al. (2018) Simulating the Last Interglacial Greenland stable water isotope peak: The role of Arctic sea ice changes. *Quaternary Science Reviews*, 198. pp. 1-14. ISSN: 0277-3791

<https://doi.org/10.1016/j.quascirev.2018.07.027>

(c) 2018 Elsevier Ltd. This manuscript version is made available under the CC BY-NC-ND 4.0 license <https://creativecommons.org/licenses/by-nc-nd/4.0/>

Reuse

This article is distributed under the terms of the Creative Commons Attribution-NonCommercial-NoDerivs (CC BY-NC-ND) licence. This licence only allows you to download this work and share it with others as long as you credit the authors, but you can't change the article in any way or use it commercially. More information and the full terms of the licence here: <https://creativecommons.org/licenses/>

Takedown

If you consider content in White Rose Research Online to be in breach of UK law, please notify us by emailing eprints@whiterose.ac.uk including the URL of the record and the reason for the withdrawal request.

1 **Simulating the Last Interglacial Greenland stable water**
2 **isotope peak: the role of Arctic sea ice changes**

3 **Irene Malmierca-Vallet ^{a, b}, Louise C. Sime ^a, Julia C. Tindall ^c, Emilie Capron ^{a, d}, Paul J.**
4 **Valdes ^b, Bo M. Vinther ^d, Max D. Holloway ^a**

5 ^a British Antarctic Survey, High Cross, Madingley Road, Cambridge, CB3 0ET, UK

6 ^b School of Geographical Sciences, University of Bristol, University Road, Bristol, BS8 1SS, UK

7 ^c School of Earth and Environment, University of Leeds, Leeds, LS2 9JT, UK

8 ^d Centre for Ice and Climate, Niels Bohr Institute, University of Copenhagen, Juliane Maries Vej 30,
9 DK-2900, Copenhagen, Denmark

10 **Abstract**

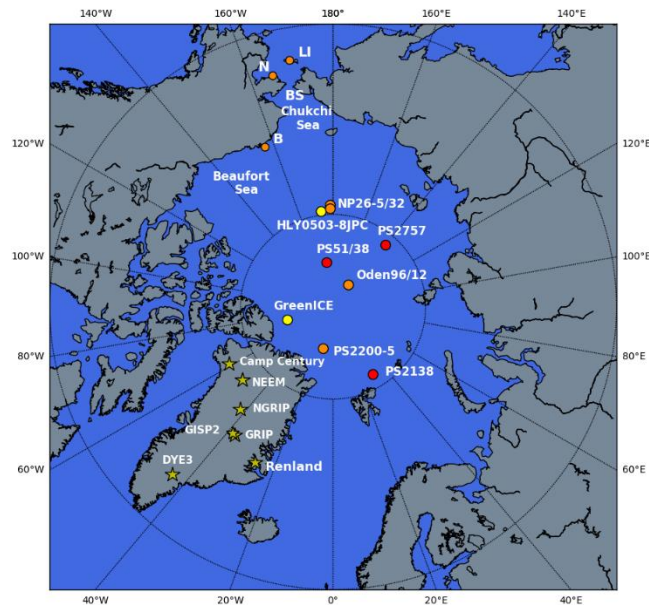
11 Last Interglacial (LIG), stable water isotope values ($\delta^{18}\text{O}$) measured in Greenland deep ice
12 cores are at least 2.5‰ higher compared to the present day. Previous isotopic climate
13 simulations of the LIG do not capture the observed Greenland $\delta^{18}\text{O}$ increases. Here, we use the
14 isotope-enabled HadCM3 (UK Met Office coupled atmosphere-ocean general circulation
15 model) to investigate whether a retreat of Northern Hemisphere sea ice was responsible for this
16 model-data disagreement. Our results highlight the potential significance of sea ice changes on
17 the LIG Greenland isotopic maximum. Sea ice loss in combination with increased sea surface
18 temperatures, over the Arctic, affect $\delta^{18}\text{O}$: water vapour enriched in heavy isotopes and a
19 shorter distillation path may both increase $\delta^{18}\text{O}$ values over Greenland. We show, for the first
20 time, that simulations of the response to Arctic sea ice reduction are capable of producing the
21 likely magnitude of LIG $\delta^{18}\text{O}$ increases at NEEM, NGRIP, GIPS2 and Camp Century ice core
22 sites. However, we may underestimate $\delta^{18}\text{O}$ changes at the Renland, DYE3 and GRIP ice core
23 locations. Accounting for possible ice sheet changes is likely to be required to produce a better
24 fit to the ice core measurements.

25 **1. Introduction**

26 Polar Regions are especially sensitive to variations in radiative forcing; they can act as
27 amplifiers of climate change via albedo feedbacks (e.g. Vaughan et al., 2013). Studying these
28 climate feedback processes is fundamental for better understanding future high-latitude
29 responses to increasing greenhouse gas (GHG) emissions. Past warm periods like the Last
30 Interglacial (LIG, approximately 129 - 116 thousand of years BP, hereafter ka) provide an ideal
31 case study to evaluate the capability of climate models to appropriately capture processes
32 involved in polar amplification (e.g. Otto-Bliesner et al., 2013; Schmidt et al., 2014).

33 During the LIG, large parts of the Earth showed warmer conditions compared to present day
34 (e.g. CAPE Last Interglacial Project Members, 2006; Turney and Jones, 2010). The increase
35 in summertime insolation at northern high latitudes contributed to a warmer-than-present-day
36 Arctic region (CAPE Last Interglacial Project Members, 2006; Masson- Delmotte et al., 2013),
37 and maximum global sea level reached 6 to 9 m above present level (e.g. Dutton et al., 2015;
38 Kopp et al., 2009).

39 Little is known about the precise extent or concentration of Northern Hemisphere (NH) sea ice
40 during the LIG. Figure 1 and supplementary table 1 show the sparse set of available
41 observations of NH sea ice changes for the LIG. As recent data compilations show that high
42 northern latitude surface air temperatures (SATs) and sea surface temperatures (SSTs) were
43 warmer in the LIG (Capron et al., 2014, 2017; Hoffman et al., 2017), it is probable that there
44 was both reduced winter and summer sea ice extent compared to today. This is supported by
45 marine cores located in the Arctic Ocean (figure 1 : GreenICE and HLY0503-8JPC cores)
46 which show planktonic foraminifers characteristic of subpolar, seasonally open waters were
47 present at these sites during the LIG, possibly reflecting ice free summer conditions in the
48 central LIG Arctic Ocean.



49

50 **Figure 1.** Map of the Arctic Ocean showing the position of observations of sea ice change based on
 51 subpolar foraminifers (yellow circles), mollusc and ostracode faunas (orange circles) and biomarker
 52 proxy IP25 (red circles). Also indicated are key regions: St Lawrence Island (LI), Nome (N), Bering
 53 Strait (BS), Barrow (B). Also shown are Greenland ice cores (yellow stars) which contain LIG ice:
 54 NEEM (77.5°N, 51.1°W), NGRIP (75.1°N, 42.3°W), GRIP (72.6°N, 37.6°W), GISP2 (72.6°N,
 55 38.5°W), Renland (71.3°N, 26.7°W), DYE3 (65.2°N, 43.8°W) and Camp Century (77.2°N 61.1°W).

56 In addition, LIG deposits on the Chukchi Sea coast include fossils of species presently known
 57 to be limited to the warmer northwest Pacific, while intertidal snails retrieved close to Nome
 58 suggest annually ice-free conditions around the coast south of the currently seasonally ice
 59 covered Bering Strait (Brigham-Grette and Hopkins, 1995; Brigham-Grette et al., 2001).
 60 Deposits close to Barrow contain some ostracode species that are only found today in the North
 61 Atlantic and deposits on the Alaskan Coastal Plain indicate that several mollusc species
 62 expanded their range well into the Beaufort Sea (Brigham-Grette and Hopkins, 1995). The
 63 nature of marine faunas at St. Lawrence Island, Beaufort Sea shelf and Nome suggests that
 64 winter sea ice did not expand south of Bering Strait, and that the Bering Sea was annually ice-
 65 free (Brigham-Grette and Hopkins, 1995) (figure 1 and supplementary table 1). Additionally,
 66 the ostracode sea ice proxy of Cronin et al. (2010) (figure 1 : NP26-5/32, Oden96/12-1pc and
 67 PS2200-5 cores) agree with the idea of sea ice glacial-interglacial variability, with sea-ice
 68 maximum on the Morris Jesup Rise and the Lomonosov and Mendelejev Ridges during

69 interglacial-to-glacial transitions and minimum coverage during peak interglacial periods (e.g.
70 MIS 5e) (supplementary table 1).

71 In a recent study, a more direct sea ice proxy named “IP25” is used in combination with
72 terrestrial and open-water phytoplankton biomarkers to reconstruct the Arctic sea ice
73 distribution during the LIG (Stein et al., 2017). The authors propose relatively closed sea ice
74 cover conditions over PS2757-8 core (figure 1 and supplementary table 1), possibly ice-free
75 conditions in the direction of the East Siberian shelf and significantly reduced sea ice cover
76 over the Barents Sea continental margin (figure 1: PS2138-2 core). In contrast to previous
77 studies (e.g. Adler et al. 2009), that point to an Arctic Ocean perhaps free of summer sea ice,
78 Stein et al. (2017) indicate the presence of perennial sea ice in two cores from central Arctic
79 Ocean during MIS 5e (figure 1: PS2200-5 and PS51/038-3 cores). Note, however, planktonic
80 foraminifers were also present at these two sites (PS2200-5 and PS51/038-3) during the LIG,
81 possibly reflecting phases of summer open-water conditions to allow foraminifers to reproduce
82 (Spielhagen et al., 2004).

83 Measurements of stable water isotopes, $\delta^{18}\text{O}$ and δD , in ice cores yield useful information on
84 past temperature changes. High-latitude local temperature is a principal control on the
85 distribution of $\delta^{18}\text{O}$ and δD in preserved Greenland ice (Dansgaard, 1964). Originally, $\delta^{18}\text{O}$
86 measurements have been translated into temperature making use of a linear relationship ($\delta^{18}\text{O}$
87 = $aT+b$, T being surface temperature) obtained from spatial information (e.g. Dansgaard, 1964;
88 Jouzel et al., 1994, 1997). However, over the last decades, it has become evident that this
89 isotope-temperature relationship is affected by atmospheric transport, evaporation conditions
90 and precipitation intermittency, and therefore varies in both space and time (e.g. Jouzel et al.,
91 1997; Masson-Delmotte et al., 2011). By influencing these key aspects, sea ice condition
92 changes have been proposed to exert significant control over the distribution of isotopes in

93 polar ice (e.g. Holloway et al., 2016a; Holloway et al., 2017; Rehfeld et al., 2018; Sime et al.,
94 2013).

95 LIG ice layers have been found in numerous Greenland deep ice cores (figure 1) (e.g. NGRIP
96 Project Members, 2004; NEEM community members, 2013; Landais et al., 2016 for a review).
97 The LIG $\delta^{18}\text{O}$ anomaly estimated at the initial snowfall NEEM deposition site (value of 3.6‰
98 at 126 ka) was translated into precipitation-weighted surface temperatures $7.5 \pm 1.8^\circ\text{C}$ warmer
99 compared to the last millennium and $+8 \pm 4^\circ\text{C}$ when accounting for Greenland ice sheet
100 elevation changes and upstream effects (NEEM community members, 2013). LIG climate
101 simulations in response to GHG and orbital forcing alone fail to capture these anomalies for
102 both $\delta^{18}\text{O}$ and temperature (e.g. Lunt et al., 2013; Masson-Delmotte et al., 2013; Otto-Bliesner
103 et al., 2013; Sjolte et al., 2014). Recent sensitivity studies show that changes in the GIS
104 topography and sea ice retreat in the Nordic Seas can lead to enhanced surface warming (up to
105 5°C) in northwest Greenland, reducing the mismatch between models and data (Merz et al.,
106 2014a, 2016).

107 Whereas the temperature profile measured in the borehole can be used to calibrate the Holocene
108 isotope-temperature slope (Vinther et al., 2009), this is not possible for the LIG as
109 palaeotemperatures for this period are not conserved in the ice sheet. This means that, the use
110 of isotopically enabled General Circulation Models (GCMs) is probably the best available
111 method to constrain the LIG isotope-temperature slope (e.g. Sime et al., 2013; Sjolte et al.,
112 2014). Previous isotopic climate simulations of the LIG underestimate the $\delta^{18}\text{O}$ anomalies of
113 $\sim +3\text{‰}$ observed in Greenland ice cores (Masson-Delmotte et al., 2011; Sjolte et al., 2014). An
114 exception is the study carried out by Sime et al. (2013) where Greenland $\delta^{18}\text{O}$ anomalies of
115 $>3\text{‰}$ are simulated over central Greenland. Note, however, that Sime et al. (2013) use GHG-
116 forced simulations as analogies for the LIG climate which could be problematic because the

117 climate response to the anthropogenic forcing projected for the near future is essentially
118 different from the climate response to the orbital forcing characteristic of the LIG warmth.

119 Here we therefore aim to better understand the processes behind the LIG Greenland isotope
120 peak. In particular, we investigate whether a retreat of NH sea ice could have been responsible
121 for the Greenland isotopic maximum. Thus, we design a set of LIG sea ice sensitivity
122 experiments that complement previous modelling studies with the detailed investigation of the
123 role of NH sea ice changes on LIG isotopic simulations.

124 In overview, we first describe the isotopic model and explain the design of the LIG sea ice
125 sensitivity experiments. Secondly, we compile LIG Greenland isotopic as well as Arctic and
126 Atlantic sea surface observations. Third, we analyse the modelled NH anomalies for $\delta^{18}\text{O}$ and
127 temperature and discuss the response of the hydrological cycle to sea ice retreat. Finally, we
128 summarise our findings and draw together some conclusions.

129 **2. Methods**

130 **2.1. Model description**

131 In order to investigate the isotopic response to a retreat of NH sea ice, we use the isotope-
132 enabled HadCM3 (Hadley Centre Coupled Model Version 3); a UK Met Office coupled
133 atmosphere-ocean GCM. The horizontal grid spacing of the atmosphere component is 2.5°
134 (latitude) by 3.75° (longitude) with 19 vertical levels (Gordon et al., 2000). The ocean
135 component has a horizontal grid resolution of 1.25° by 1.25° and has 20 vertical levels (Gordon
136 et al., 2000). In addition to the ocean and atmosphere components, HadCM3 also includes sea
137 ice and vegetation components (Gordon et al., 2000). We use the TRIFFID (Top-down
138 Representation of Interactive Foliage and Flora Including Dynamics) dynamic global
139 vegetation model and the MOSES 2.1 land surface scheme where energy and water fluxes
140 between the surface and the atmosphere are calculated.

141 HadCM3 has been used to investigate the Last Glacial Maximum (Holloway et al., 2016b),
142 past warm intervals (Holloway et al., 2016a; Tindall and Haywood, 2015), as well as present
143 day (Tindall et al., 2009). The representation of the distribution of isotopes in the atmosphere
144 and ocean shown by the model is reasonable (Tindall et al., 2009, 2010) (see Appendix A
145 for a more detailed description of how HadCM3 performs across Greenland).

146 **2.2. Experimental setup – isotopic simulations**

147 HadCM3 is used to simulate the isotopic response to different sea ice retreat scenarios. We
148 perform snapshot simulations, representative of 125 ka conditions. All LIG climate model
149 simulations are driven with greenhouse gas concentrations and orbital parameters for 125 ka
150 and compared to a pre-industrial (PI) control experiment, driven with greenhouse gas values
151 and orbital parameters for 1850-years before present (BP). All experiments are run with a pre-
152 industrial ice-sheet distribution (US Navy 10' dataset - see unified model documentation No 70
153 by Jones, 1995). Each of the 70-year long LIG sea ice sensitivity experiments are continued
154 from a 200-year long spin-up of a 125 ka control simulation. The 200-year long spin up ensures
155 quasi-equilibrium conditions between the atmosphere and the upper ocean.

156 To test whether NH sea ice retreat was responsible for the Greenland LIG isotope peak, we
157 perform a suite of experiments each with a different reduction in Arctic sea ice extent. To
158 generate the sea ice retreats, we apply the same method previously used by Holloway et al.
159 (2016a) and implement heat fluxes (from 0 W m^{-2} up to 300 W m^{-2}) to the bottom of the NH
160 sea ice. No other effects are applied to the model physics. That is, the sea ice specific heat flux
161 forcing is kept constant during the whole annual cycle, so the seasonal cycle of sea ice decay
162 and growth is still calculated by the model. The atmosphere and ocean components respond to
163 sea ice variations and sea ice thus changes over time with the coupled model. A full list of
164 experiments is shown in supplementary table 2. A total of 22 experiments have been conducted
165 with different sea ice scenarios each forced by a sea ice heat flux from between 0 to 300 W m^{-2}

166 ². This approach explores the impact of forced arctic sea ice changes on the $\delta^{18}\text{O}$ signal across
167 Greenland.

168 **2.3. Model-Data Comparison**

169 **2.3.1. Greenland ice core data**

170 To evaluate the impact of different sea ice configurations on the $\delta^{18}\text{O}$ ice core record, the model
171 results are compared to the $\delta^{18}\text{O}$ values in LIG ice layers. These layers have been identified
172 near the bedrock of seven Greenland deep ice cores: NEEM (NEEM community members,
173 2013), NGRIP (NGRIP members, 2004), GISP2 (Grootes et al., 1993), GRIP (GRIP members,
174 1993), Camp Century (Dansgaard et al., 1969), Renland (Johnsen et al., 2001) and DYE-3
175 (Dansgaard et al., 1982) (Johnsen and Vinther, 2007; NEEM community members, 2013;
176 figure 1 and table 3).

177 The bottom of the DYE-3, Camp Century, Renland, GRIP and GISP2 ice cores is affected by
178 stratigraphic disturbances and cannot be unambiguously datable (e.g. Johnsen et al. 2001;
179 Grootes et al. 1993; Landais et al. 2003). While the NGRIP core does not cover the entire LIG,
180 its stratigraphy is believed to be well preserved all the way to bedrock due to melting at bed
181 (NGRIP members 2004). Peak NGRIP LIG $\delta^{18}\text{O}_{\text{ice}}$ values were 3.1‰ higher than present day
182 (Johnsen and Vinther 2007).

183 The recent deep drilling at NEEM yielded an 80 m section of ice in stratigraphic order, in
184 between disturbed layers. It extends the Greenland $\delta^{18}\text{O}$ record back to ~128.5 ka (NEEM
185 community members, 2013). At 126 ka, $\delta^{18}\text{O}_{\text{ice}}$ values were estimated to be 3.6‰ higher than
186 preindustrial local values at the NEEM deposition site (around 205±20 km upstream of the
187 NEEM drilling site; NEEM community members, 2013). The NEEM community members
188 (2013) used the Holocene isotope-temperature relationship of 0.5 ‰/°C (calibrated using
189 borehole temperature data from other Greenland ice cores; Vinther et al., 2009) to translate the

190 3.6‰ anomaly into a local warming of 7.5 ± 1.8 °C. After accounting for ice sheet elevation
191 changes and upstream effects, this resulted in a reconstruction of a 8 ± 4 °C warming compared
192 to the last millennium (NEEM community members, 2013). Using an alternative method based
193 on measurements of the ice core air isotopic composition ($\delta^{15}\text{N}$), Landais et al. (2016) deduce
194 a similar surface temperature warming at NEEM of 8 ± 2.5 °C at 126 ka. Note that this latter
195 estimate does not account for ice sheet altitude changes.

196 **2.3.2. Sea surface temperature observations**

197 Syntheses of maximum LIG surface temperature based on ice, marine and terrestrial archives
198 (Turney and Jones, 2010; McKay et al. 2011) have been until recently used for model
199 evaluation (e.g. Lunt et al. 2013, Sime et al. 2013). However given that the warming was not
200 synchronous globally (e.g. Govin et al. 2012, Bauch and Erlenkeuser, 2008), these syntheses
201 do not provide a realistic representation of the LIG climate nor a specific time slice.

202 More recent compilations by Capron et al. (2014) and Hoffman et al. (2017) have developed
203 harmonized chronologies for paleoclimatic records to produce a spatio-temporal representation
204 of the LIG climate. Capron et al. (2014; 2017) produced five 2000 year long time slices of
205 high-latitude (above 60°N and 60°S) air and sea surface temperature anomalies centred on 115,
206 120, 125, 127 and 130 ka. Hoffman et al. (2017) provide time slices of global extent of SST
207 anomalies at 120, 125 and 129 ka. While Capron et al. (2014) gather mainly summer high-
208 latitude SST records, Hoffman et al. (2017) provide annual and summer SST records extending
209 down to the tropics. These two datasets use different reference chronologies and distinct
210 methodologies to deduce temporal surface temperature changes and therefore, should be used
211 as independent data benchmarks (Capron et al., 2017).

212 Here, we compare our model results with the LIG SST datasets compiled for the time interval
213 125 ka by Capron et al. (2014) and Hoffman et al. (2017) in the high latitude regions. In order

214 to determine the degree of agreement between model results and data, we calculate the root
215 mean square error (RMSE). We do not consider this analysis as an ideal skill score owing to
216 uneven data coverage. Nevertheless, it provides a first-order estimate of the ability of the model
217 to replicate the observations.

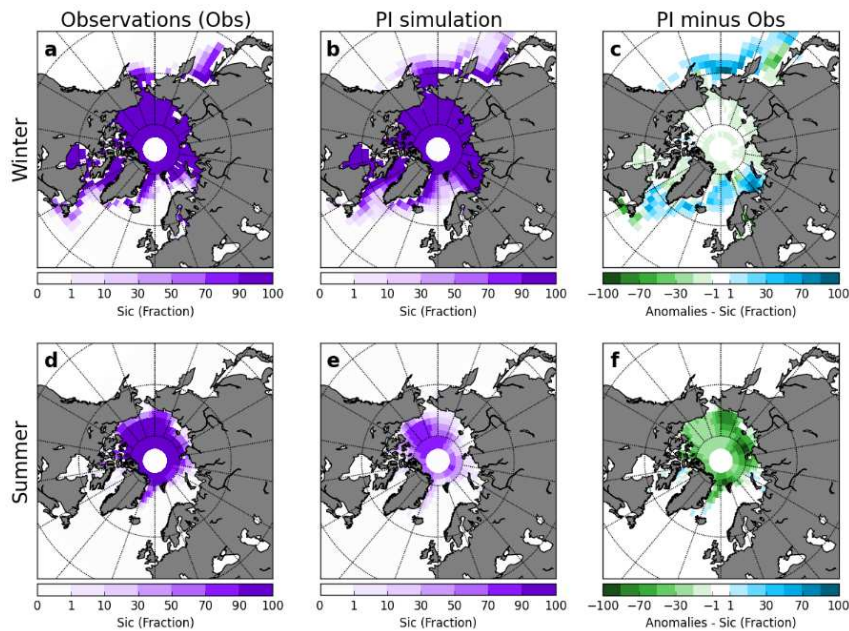
218 **3. Isotopic simulation results**

219 We present results from 22 sea ice scenarios here; In each case climatological averages are
220 determined considering the last 50 years of the simulations and a two-sided Student's t test is
221 used to assess the statistical significant of changes (e.g. von Storch and Zwiers, 2001). In
222 addition we focus on three example scenarios which depict low, medium and high sea ice loss.
223 The example experiments show a winter sea ice reduction (hereafter WSIR) compared to the
224 PI simulation of 7% (WSIR-7), 35% (WSIR-35), and 94% (WSIR-94) (experiments marked in
225 red in supplementary table 2).

226 **3.1. Model performance**

227 We start the results section by reviewing the model sea ice output over the Arctic Ocean. Figure
228 2 shows the comparison of the PI simulation to gridded observational sea ice data (Meier et al.,
229 2017 and Peng et al., 2013). HadCM3 simulates too little summer sea ice under PI conditions
230 (figure 2f). Over the Labrador, Norwegian, Barents and Bering seas, the comparison reveals
231 too much winter sea ice under PI conditions (figure 2c). The model-data mismatch may partly
232 be attributed to the model sea ice physics. Although HadCM3 produces a fairly realistic
233 simulation of sea ice (as previously described by Gordon et al., 2000), the ice pack is
234 represented by a single ice-thickness category and sea ice dynamics are modelled in a rather
235 simple manner (e.g., sea ice is advected via the ocean surface currents) compared to more recent
236 sea ice models (e.g. CICE sea-ice model). Furthermore, the difference between the modern
237 reference (1979 – 1989 AD) used for the data and the PI reference used for the model may also

238 contribute to the discrepancies between model output and data. For example, during the pre-
 239 industrial era, the lower GHG emissions relative to the period 1979-1989 (IPCC, 2013), may
 240 have allowed more extensive winter sea ice cover.



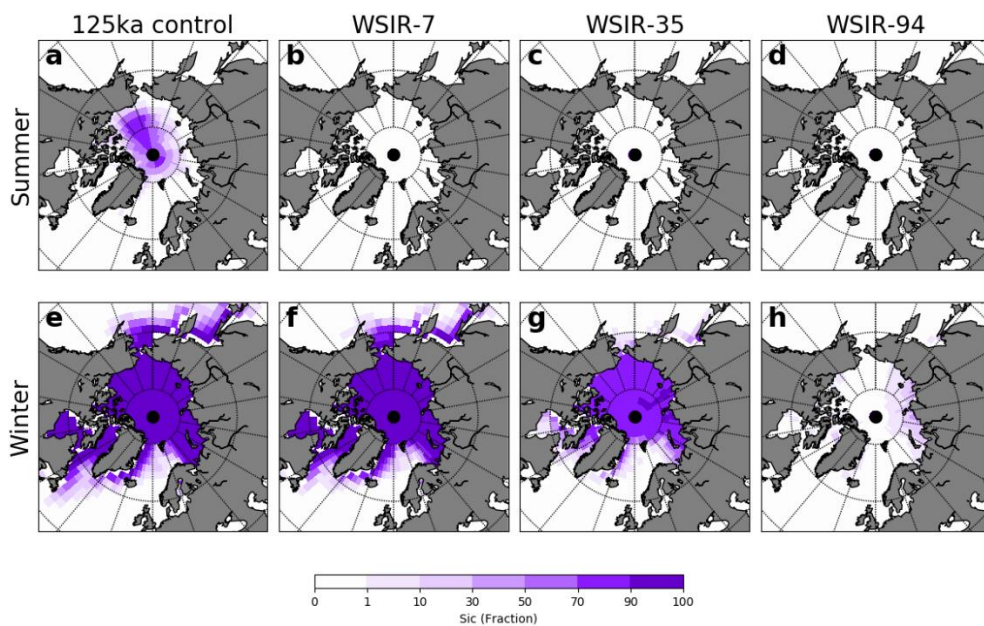
241
 242 **Figure 2.** Comparison of the PI simulation to gridded observational sea ice data. Observational data
 243 for: (a) winter (March) and (d) summer (September) sea ice concentration (Meier et al., 2017 and
 244 Peng et al., 2013). In particular, we use the Goddard Merged sea ice record from 1979 to 1989 (see
 245 Meier et al., 2017 and Peng et al., 2013 for more information about the sea ice data). Simulated sea
 246 ice concentration for: (b) winter (March) and (e) summer (September) under PI conditions. (c) and
 247 (f) show anomalies (PI minus observations) for winter and summer respectively.

248 **3.2. Sea ice extent**

249 For this analysis, we use the standard definition of sea ice extent: the ocean area where sea ice
 250 concentration (sic) is at least 15%. Plots of the September and March Arctic sea ice
 251 concentrations are presented in figure 3.

252 For the PI simulation, the mean annual sea ice extent is $12.77 \times 10^6 \text{ km}^2$, with a March mean
 253 of $18.90 \times 10^6 \text{ km}^2$ and a September mean of $5.43 \times 10^6 \text{ km}^2$ (table 1). The 125ka control
 254 simulation (no sea ice forcing) show a lower September mean ($4.05 \times 10^6 \text{ km}^2$ - table 1)
 255 compared to the PI experiment. This is expected because, during the LIG, larger seasonal and

256 latitudinal insolation variations at the top of the atmosphere (linked to the orbital forcing)
 257 resulted in melting of the Arctic sea ice during summer/spring (e.g. Otto-Bliesner et al., 2006).
 258 The 125 ka control simulation with no additional sea ice forcing shows a mean annual sea ice
 259 extent of $12.45 \times 10^6 \text{ km}^2$. For the LIG sea ice retreat experiments, the annual mean sea ice
 260 extent ranges from $9.19 \times 10^6 \text{ km}^2$ to $0.63 \times 10^6 \text{ km}^2$ depending on the prescribed sea ice forcing
 261 (table 1). The lowest March extent ($1.18 \times 10^6 \text{ km}^2$) is shown by the experiment with the highest
 262 sea ice forcing (WSIR-94) (table 1). To calculate the number of ice-free days per year, we
 263 consider “nearly ice-free conditions” when the extent of sea ice is less than 10^6 km^2 (IPCC AR5
 264 definition; IPCC, 2013). While the sea ice sensitivity experiments show approximately 83
 265 (WSIR-7), 205 (WSIR-35), 271 (WSIR-94) ice-free days per year, the PI and 125ka control
 266 simulations have none.



267
 268 **Figure 3.** Mean sea ice concentrations (sic - %) for September (first row) and March (second row)
 269 for the experiments: 125-ka control (a and e), WSIR-7 (b and f), WSIR-35 (c and g) and WSIR-94
 270 (d and h).

271 Supplementary figure 1d shows the annual cycle of Arctic sea ice extent in the LIG simulations.
 272 The sea ice extent amplitude is $13.47 \times 10^6 \text{ km}^2$ and $15.41 \times 10^6 \text{ km}^2$ for the PI simulation and
 273 125 ka control simulation respectively (table 1). When simulating the response to a strong sea

274 ice loss (WSIR-94), we obtain a much lower seasonal amplitude of $3.37 \times 10^6 \text{ km}^2$ (table 1).
 275 WSIR-7 and WSIR-35 experiments show sea ice extent amplitudes of $17.62 \times 10^6 \text{ km}^2$ and
 276 $12.25 \times 10^6 \text{ km}^2$ respectively (table 1).

	PI	125ka-control	WSIR-7	WSIR-35	WSIR-94
jan	15.76	16.03	14.60	8.87	2.30
feb	18.00	18.18	16.59	11.94	3.37
mar	18.90	19.46	17.62	12.25	1.18
apr	18.88	19.22	17.35	6.74	0.00
may	16.62	16.87	15.07	0.00	0.00
jun	13.85	13.70	9.93	0.00	0.00
jul	9.54	8.06	1.71	0.00	0.00
aug	6.08	4.59	0.00	0.00	0.00
sep	5.43	4.05	0.00	0.00	0.00
oct	6.53	5.67	0.00	0.00	0.00
nov	10.47	10.25	5.82	0.10	0.06
dec	13.20	13.30	11.58	1.41	0.68
Mean annual extent	12.77	12.45	9.19	3.44	0.63
Extent amplitude	13.47	15.41	17.62	12.25	3.37

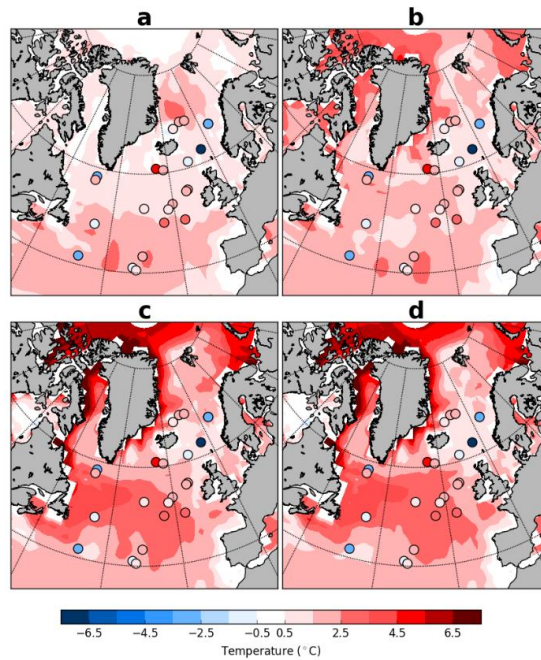
277 **Table 1.** Monthly and annual mean sea ice extent and amplitude of sea ice extent (maximum minus
 278 minimum annual sea ice extent) for the PI and selected LIG simulations. Values expressed in 10^6 km^2 .

279 **3.3. Sea surface and surface air temperatures**

280 For the 125 ka control simulation with no additional sea ice forcing, there is an increase of NH
 281 summer (June-July-August - JJA) temperatures compared to the PI simulation (local increases
 282 exceed 3°C – supplementary figure 2c). All sea ice loss experiments reveal an Arctic warming
 283 all year round despite reduced winter insolation (supplementary figure 2d to 2l). The Arctic
 284 warming, which peaks during the winter months (December-January-February – DJF)
 285 (supplementary figure 2e, 2h and 2k), is associated with sea ice retreat, through warmer,
 286 expanded ocean waters leading to a warmer atmosphere. This warming impacts the entire
 287 circumpolar region, including Greenland.

288 The large precipitation-weighted air temperature signal reconstructed at the NEEM
 289 depositional site of $+7.5 \pm 1.8^\circ\text{C}$ ($8 \pm 4^\circ\text{C}$ when accounting for GIS elevation changes) is not
 290 reproduced by any of our LIG simulations. At the NEEM deposition site, the experiments

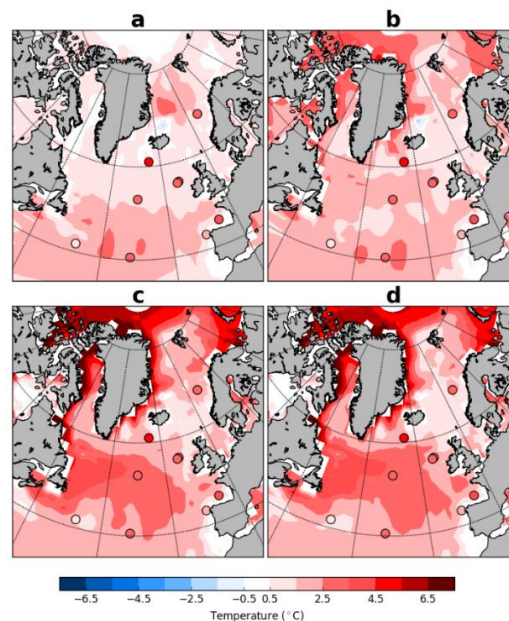
291 WSIR-7, WSIR-35 and WSIR-94 show precipitation-weighted SAT anomalies of 2.5°C,
 292 3.5°C, 3.0°C respectively, whereas the 125 ka control simulation reveals a more modest
 293 warming of 2.1°C relative to the PI control experiment. This underestimation in models of the
 294 LIG warming is a discrepancy that has already been extensively discussed in previous studies
 295 (e.g. Lunt et al., 2013; Sime et al., 2013).



296
 297 **Figure 4.** The 125 ka data-based time slice (dots) provided by Capron et al. (2014) superimposed
 298 onto modelled summer (JAS) SST anomalies relative to the PI simulation for: (a) 125ka-control
 299 (RMSE = 3.0), (b) WSIR-7 (RMSE = 3.0), (c) WSIR-35 (RMSE = 3.2) and (d) WSIR-94 (RMSE =
 300 3.2).

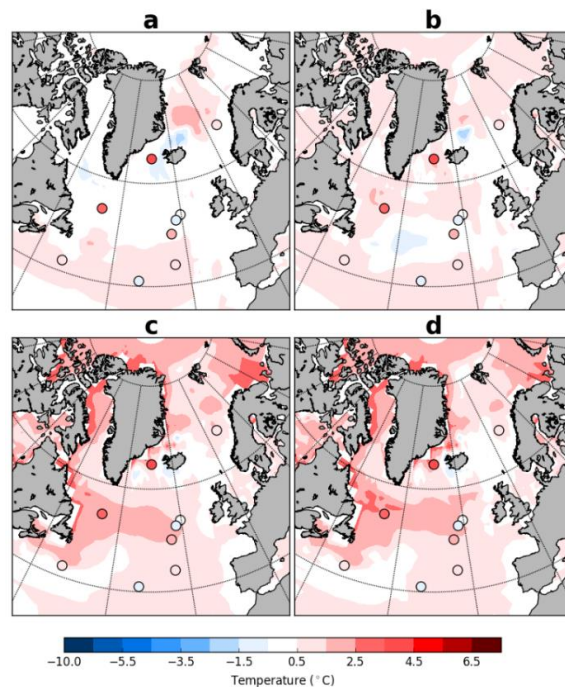
301 Figure 4 shows results from the 125 ka simulations compared with the 125 ka time slice of
 302 Capron et al. (2014). Simulated summer SST anomalies are defined as July-August-September
 303 (JAS) to be in agreement with the data of Capron et al. (2014). Considering the uncertainties
 304 on SST estimates ($\pm 2.6^\circ\text{C}$ on average, see Capron et al., 2014, 2017 for 2σ uncertainty
 305 estimates of individual records), the match between the model simulation with no additional
 306 sea ice forcing and data is reasonable (figure 4a). When the response to a forced retreat of sea
 307 ice is simulated, the agreement with data is very similar than if no sea ice forcing is applied
 308 (figure 4b, 4c and 4d). We obtain similar values of RMSE for NH SSTs for all simulations

309 regardless of the sea ice forcing (figure 4). The experiments WSIR-94 and WSIR-35 show the
 310 highest RMSE (3.2°C), whereas the 125ka-control and WSIR-7 simulations have the lowest
 311 (“best”) RMSE (3.0°C) (figure 4). Nevertheless, all simulations fail to reproduce the
 312 reconstructed SST anomalies at the sites characterised by cooler-than-present-day conditions
 313 irrespective of the sea ice forcing (figure 4). These are located in the Norwegian Sea and in the
 314 region south of Greenland. Previous modelling studies (e.g. Capron et al., 2014; Pedersen et
 315 al., 2016a) have also difficulties to capture this cooling trend over these regions. Bauch et al.
 316 (2012) propose a reduced Atlantic Ocean heat transfer to the LIG Arctic which could explain
 317 the regional cooling over the Nordic Seas. And, Langebroek and Nisancioglu (2014) simulate
 318 (with the Norwegian Earth System Model - NorESM) cooling conditions over central North
 319 Atlantic and Nordic Seas for the LIG, suggesting the simulated climate over these areas may
 320 be model dependent.



321
 322 **Figure 5.** The 125 ka data-based time slice (dots) provided by Hoffman et al. (2017) superimposed
 323 onto modelled summer (JAS) SST anomalies relative to PI simulation for: (a) 125ka-control (RMSE
 324 = 2.3), (b) WSIR-7 (RMSE = 1.9), (c) WSIR-35 (RMSE = 1.5) and (d) WSIR-94 (RMSE = 1.4).
 325 Due to its coastal proximity we exclude MD95-2040 site from our model-data analysis. See
 326 Hoffman et al, 2017 for additional information.

327 In addition, the model results are compared with the 125 time slice from the Hoffman et al.
 328 (2017) synthesis. All LIG simulations are generally in good agreement with both summer and
 329 annual SST data, considering the uncertainty range related to SST estimates (see Hoffman et
 330 al., 2017 for 2σ uncertainty estimates of individual records) (figure 5 and 6). While the
 331 experiments with medium and strong sea ice forcing (WSIR-35 and WSIR-94) show the lowest
 332 RMSE values (“best” model-data agreement) for both summer (RMSE = 1.5°C and 1.4°C
 333 respectively) and annual (RMSE = 1.5°C and 1.4°C respectively) SSTs, the 125ka control
 334 simulation reveals the highest RMSE values (2.3°C and 1.9°C for summer and annual SSTs
 335 respectively) (figure 5 and 6).

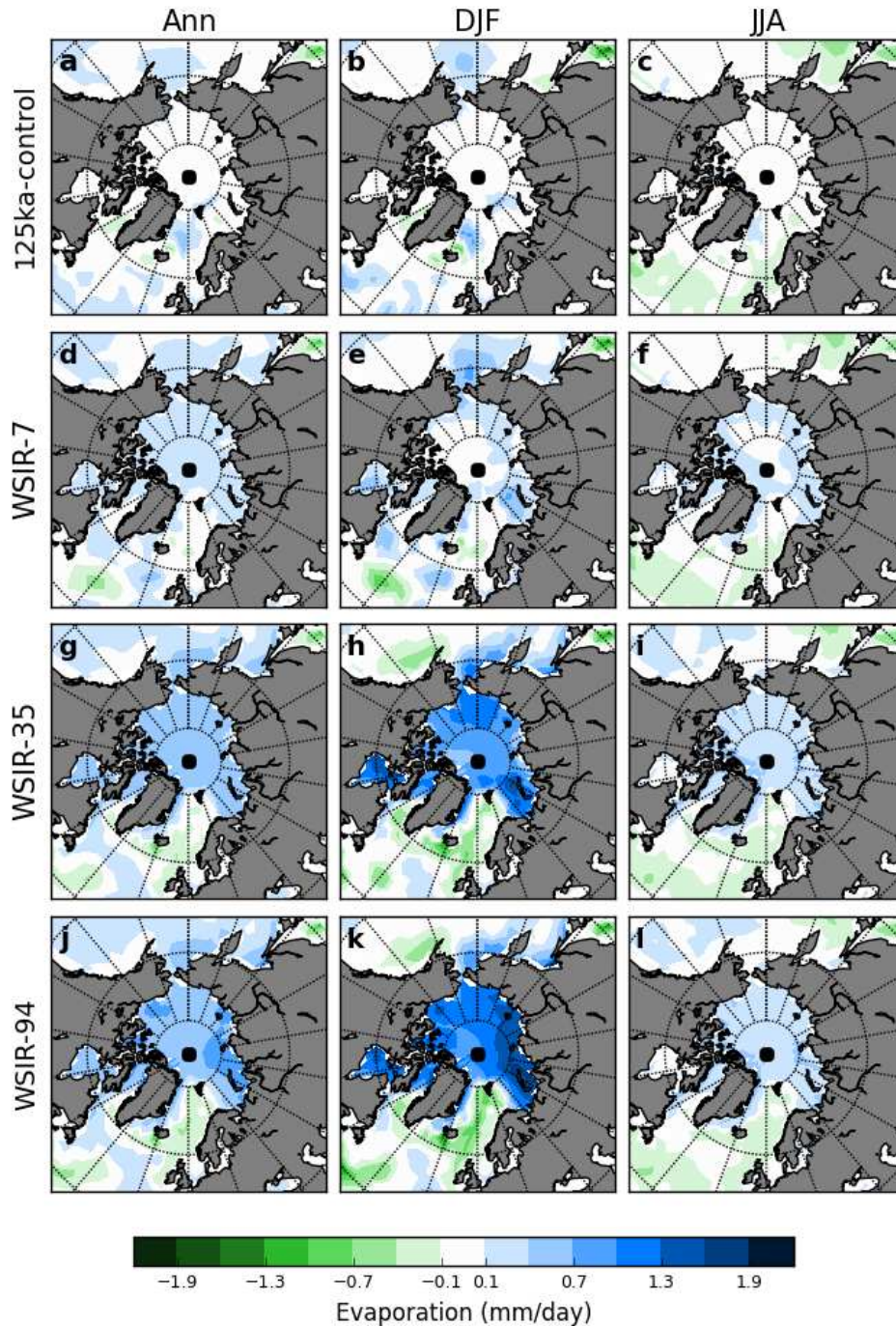


336
 337 **Figure 6.** The 125 ka data-based time slice (dots) provided by Hoffman et al. (2017) superimposed
 338 onto modelled annual SST anomalies relative to PI simulation for: (a) 125ka-control (RMSE = 1.9),
 339 (b) WSIR-7 (RMSE = 1.5), (c) WSIR-35 (RMSE = 1.5) and (d) WSIR-94 (RMSE = 1.4). Due to its
 340 coastal proximity we exclude MD95-2040 site from our model-data analysis. See Hoffman et al,
 341 2017 for additional information.

342 **3.4. Response of the hydrological cycle to the sea ice retreat**

343 Annual, winter (DJF) and summer (JJA) averages of Arctic evaporation are shown in figure 7.
 344 Directly over areas of reduced Arctic sea ice cover, simulations show an increase in

345 evaporation. Over the Arctic Ocean, all sea ice reduction experiments show an increase in
 346 evaporation during both summer and winter compared to the PI simulation (figure 7). When
 347 sea ice melts, the replacement of ice at temperatures below zero by open waters, results in a
 348 significant increase in evaporation, particularly during the winter months (figure 7h and 7k).



349
 350
 351
 352
 353

Figure 7. Modelled annual (ann), summer (JJA) and winter (DJF) evaporation anomalies for the 125ka-control simulation (a to c), WSIR-7 (d to f), WSIR-35 (g to i) and WSIR-94 (j to l) compared to the PI simulation. Only the anomalies statistically significant at the 95% confidence level are displayed.

354 Over the Arctic Basin, local increases in winter evaporation rate exceed 1 mm/day in WSIR-
355 35 and 1.3 mm/day in WSIR-94, while in the low sea ice retreat scenario, WSIR-7, local
356 increases are closer to 0.4 mm/day (figure 7e, 7h, 7k).

357 The increase in evaporation rate during both summer and winter leads to an increase in
358 precipitation (supplementary figure 3). The ice retreat experiments display similar spatial
359 anomalies, particularly the rise in precipitation in the Arctic Ocean (supplementary figure 3).
360 The increases are more widespread and larger in WSIR-35 and WSIR-94 than in WSIR-7,
361 which is expected considering the larger sea ice loss (supplementary figure 3d-1). The increase
362 in precipitation is greater during the winter months than during summer when precipitation is
363 highest in the Arctic (supplementary figure 3).

364 A direct atmospheric reaction to sea ice loss and warmer SATs is a decrease in mean sea level
365 pressure (MSLP). The less stable and warmer atmosphere leads to a widespread reduction in
366 winter MSLP over the Arctic Ocean, North Pacific and Bering Sea (supplementary figure 4b-
367 d). Over the Arctic Ocean, local decreases in winter MSLP exceed 200 Pa, 650 Pa and 800 Pa
368 in WSIR-7, WSIR-35 and WSIR-94 respectively (supplementary figure 4b-d).

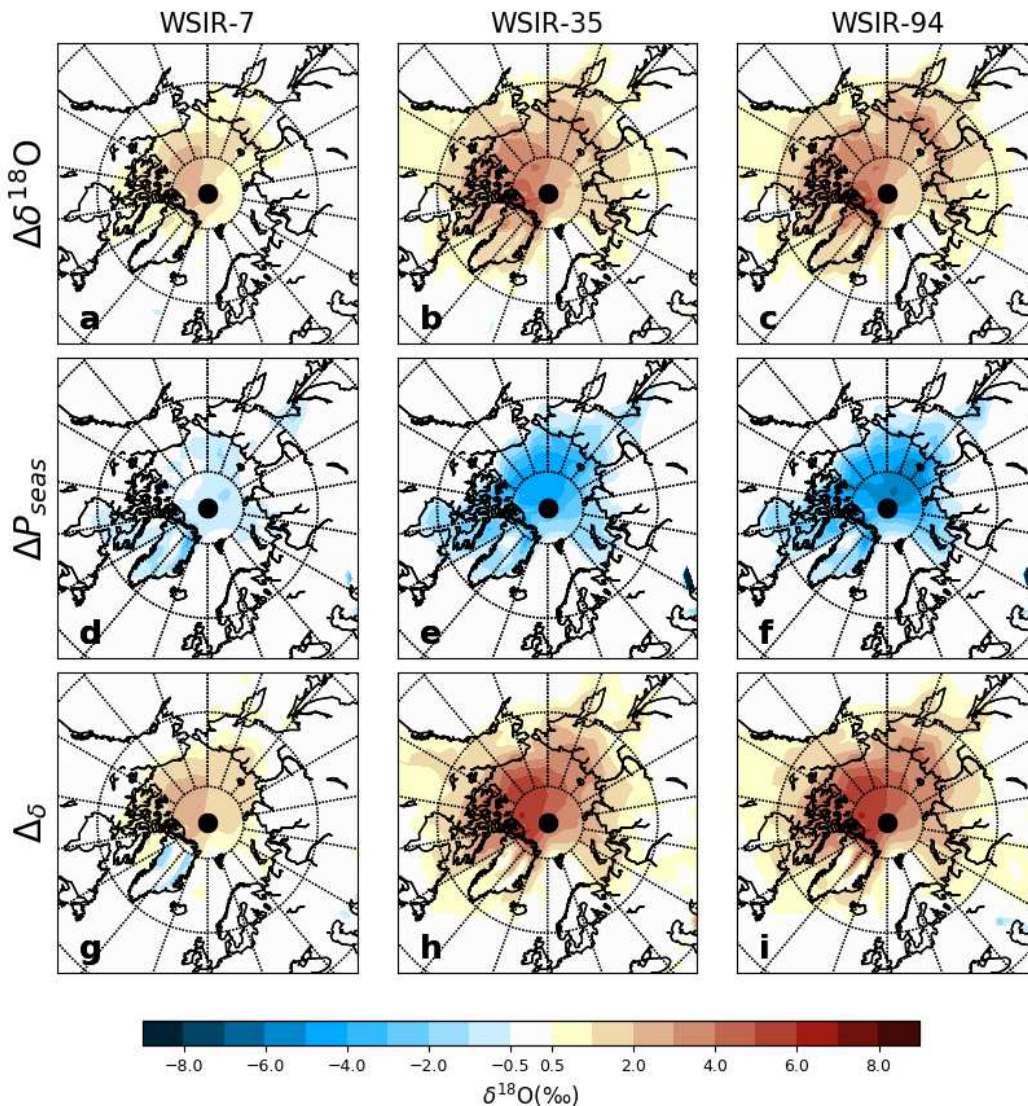
369 **3.5. Decomposition of $\delta^{18}\text{O}$ changes**

370 Ice core records reflect the deposition of snow on the surface, and therefore tend to record
371 climatic information during snow deposition events (e.g. Steig et al., 1994). Hence,
372 precipitation seasonality can cause a recording bias towards those seasons with more snowfall
373 events. Indeed, stable water isotopes in Greenland ice core records have been traditionally
374 compared with precipitation isotopic composition reproduced by isotope-enabled models (e.g.
375 Sime et al., 2013).

376 In this section, we study how changes in both the monthly isotopic composition of precipitation
 377 and the amount of monthly precipitation contribute to the simulated positive $\delta^{18}\text{O}$ anomalies at
 378 the different Greenland ice core sites (Holloway et al., 2016a; Liu and Battisti, 2015).

379 To isolate the importance of variations in the seasonal cycle of precipitation (ΔP_{seas}) to the
 380 changes in $\delta^{18}\text{O}$, we use the following decomposition:

$$381 \quad (1) \quad \Delta P_{\text{seas}} = \frac{\sum_j \delta^{18}\text{O}_j^{\text{CONT}} * P_j}{\sum_j P_j} - \frac{\sum_j \delta^{18}\text{O}_j^{\text{CONT}} * P_j^{\text{CONT}}}{\sum_j P_j^{\text{CONT}}}$$



382
 383 **Figure 8.** Decomposition of $\delta^{18}\text{O}$ changes from 125 ka sea ice retreat experiments. (a,d,g) WSIR-7;
 384 (b,e,h) WSIR-35; (c,f,i) WSIR-94. (a-c) The total change in $\delta^{18}\text{O}$ ($\Delta\delta^{18}\text{O}$). (d-f) The change due to
 385 variations in the seasonality of precipitation (ΔP_{seas}). (g-i) The change caused by variations in the
 386 $\delta^{18}\text{O}$ of precipitation ($\Delta\delta$). Anomalies are calculated compared to the 125 ka control simulation with
 387 no additional sea ice forcing.

388 Superscript CONT denote values from the 125 ka control simulation with no additional sea ice
 389 forcing and no superscript denote values from the sea ice sensitivity experiments. The relative
 390 impact of other factors (variations in the isotopic composition of precipitate and in the vapor
 391 source) contributing to the changes in $\delta^{18}\text{O}$ is quantified by:

$$392 \quad (2) \quad \Delta_{\delta} = \frac{\sum_j \delta^{18}\text{O}_j * P_j^{CONT}}{\sum_j P_j^{CONT}} - \frac{\sum_j \delta^{18}\text{O}_j^{CONT} * P_j^{CONT}}{\sum_j P_j^{CONT}}$$

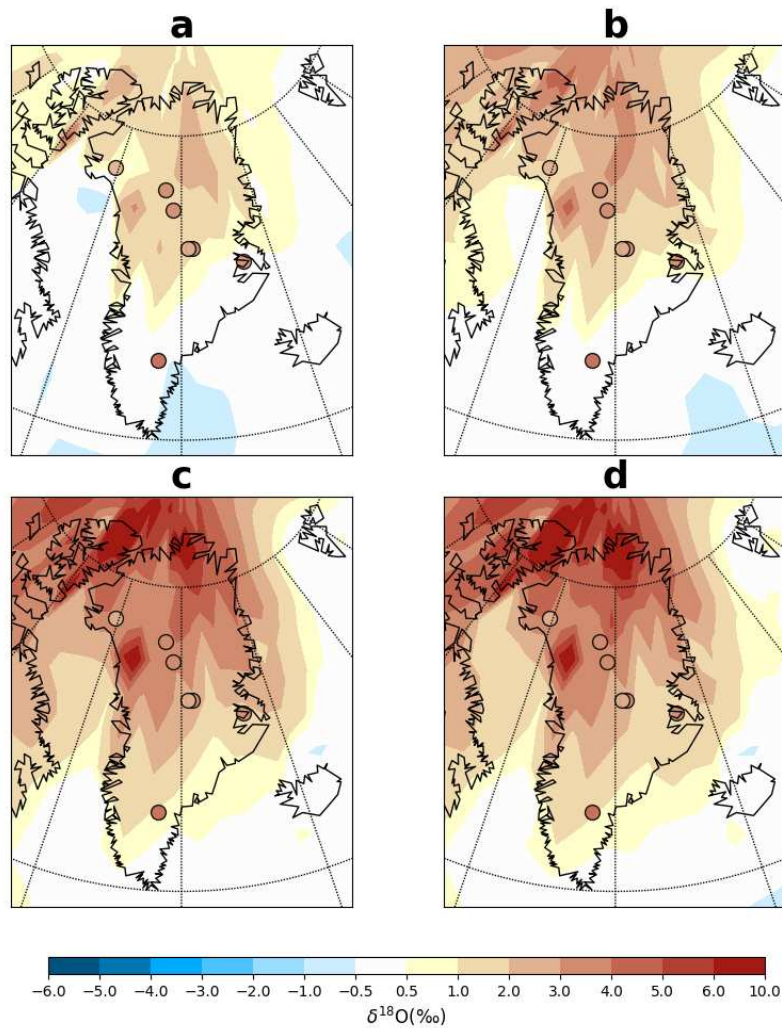
393 Using the monthly $\delta^{18}\text{O}$ from the 125 ka control simulation and the monthly precipitation of
 394 the different sea ice forcing experiments (WSIR-7, WSIR-35 and WSIR-94) (Equation 1), we
 395 determine the differences in $\delta^{18}\text{O}$ due to variations in the seasonal cycle of precipitation (figure
 396 8 d-f). In the same way, using the monthly $\delta^{18}\text{O}$ from the sea ice retreat experiments (WSIR-7,
 397 WSIR-35 and WSIR-94) and the monthly precipitation of the 125 ka control simulation
 398 (Equation 2), we isolate the effect of the variations in the isotopic composition of precipitation
 399 to the total $\delta^{18}\text{O}$ changes (figure 8 g-i).

400 For all sea ice sensitivity experiments (WSIR-7, WSIR-35 and WSIR-94), over the Arctic
 401 Ocean and Greenland, ΔP_{seas} is negative (figure 8 d-f) and Δ_{δ} is generally strongly positive
 402 (figure 8 g-i). Thus whilst more precipitation falls in the colder months under the sea ice loss
 403 scenarios, the increases in $\delta^{18}\text{O}$ related to the sea ice loss generally outweigh this impact over
 404 Greenland.

405 **3.6. Mean annual $\delta^{18}\text{O}$ changes at the NEEM deposition site**

406 At the NEEM deposition site, the 125-ka control simulation shows a precipitation-weighted
 407 $\delta^{18}\text{O}$ (hereafter $\delta^{18}\text{O}_p$) anomaly of 1.7‰ compared to the PI control simulation (figure 9a). This
 408 is too low compared to the 3.6‰ increase measured in the NEEM ice core. When the response
 409 to a forced retreat of sea ice is simulated, $\delta^{18}\text{O}_p$ anomalies rise to between 2.4‰ and 3.9‰
 410 depending on the sea ice forcing prescribed (figure 9b-d and table 2). Simulations with greater

411 than a 17% reduction in winter sea ice best fit the NEEM ice core data (considering the $\pm 1\sigma$
 412 uncertainty on the best fit curve - figure 10a).



413
 414 **Figure 9.** Observed $\delta^{18}\text{O}$ anomalies at seven Greenland ice core sites (dots) (Johnsen and Vinther,
 415 2007, NEEM community members, 2013) superimposed onto simulated annual mean precipitation-
 416 weighted $\delta^{18}\text{O}$ anomalies for: (a) 125ka-control, (b) WSIR-7, (c) WSIR-35 and (d) WSIR-94
 417 compared to the PI simulation.

Exp ID	Precipitation weighted $\delta^{18}\text{O}$ (‰)	Precipitation weighted SAT anomalies ($^{\circ}\text{C}$)	Non-weighted SAT anomalies ($^{\circ}\text{C}$)
125ka-control	1.7	2.1	0.5
WSIR-7	2.6	2.5	0.7
WSIR-11	2.5	2.9	1.1
WSIR-10	2.4	2.5	1.3
WSIR-15	3.0	3.1	1.6
WSIR-17	3.3	3.5	1.8
WSIR-17b	3.1	3.1	1.7
WSIR-19	2.9	2.6	1.6

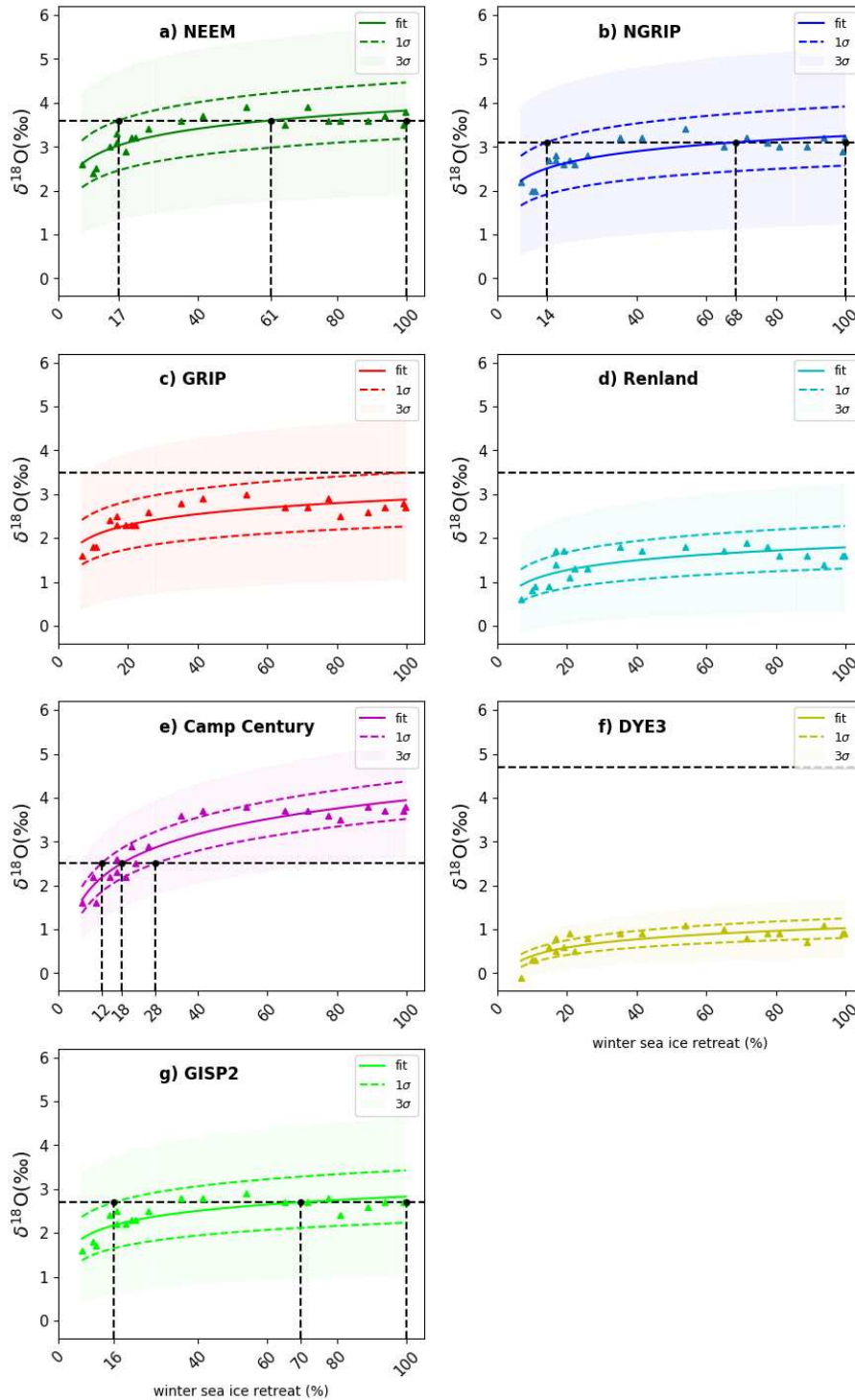
WSIR-21	3.2	3.1	1.7
WSIR-22	3.2	3.2	1.7
WSIR-26	3.4	3.0	1.7
WSIR-35	3.6	3.5	2.1
WSIR-41	3.7	3.1	2.2
WSIR-54	3.9	3.5	2.4
WSIR-65	3.5	2.8	2.3
WSIR-72	3.9	3.2	2.2
WSIR-78	3.6	2.9	2.2
WSIR-81	3.6	2.7	1.9
WSIR-89	3.6	2.8	2.1
WSIR-94	3.7	3.0	2.3
WSIR-99	3.5	2.9	2.1
WSIR-100	3.8	3.2	2.1

418 **Table 2.** Modelled annual means of precipitation-weighted $\delta^{18}\text{O}$, precipitation-weighted SAT and
419 non-weighted SAT anomalies compared to the PI simulation at the NEEM deposition site.
420 Anomalies are listed for each of the 125 ka simulations. The experiments marked in red are the ones
421 mainly discussed in the text.

422 **3.7. Mean annual $\delta^{18}\text{O}$ changes at other Greenland ice core sites**

423 The 125-ka control simulation with no additional sea ice forcing shows $\delta^{18}\text{O}_p$ anomalies of
424 1.4‰ at NGRIP and 1.1‰ at GISP2 compared to the PI control simulation (figure 9a and table
425 3). When forcing a sea ice reduction, simulated $\delta^{18}\text{O}_p$ anomalies rise to between 2.0‰ and
426 3.4‰ at NGRIP and between 1.6‰ and 2.9‰ at GISP2 depending on the sea ice forcing
427 prescribed (figure 9b-d and table 3). At NGRIP and GISP2 sites, LIG $\delta^{18}\text{O}$ values were reported
428 to be 3.1‰ and 2.7‰ higher than present day values respectively (Johnsen and Vinther 2007).
429 We find that simulations with a winter sea ice retreat higher than 14% and 16% may explain
430 the NGRIP and GISP2 data respectively (considering the $\pm 1\sigma$ uncertainty on the best fit curves
431 - figure 10b and 10g).

432 At Camp Century site, the sea ice retreat experiments show $\delta^{18}\text{O}_p$ anomalies ranging from 1.6‰
433 to 3.8‰ depending on the sea ice forcing, while the 125ka control simulation reveals a more
434 modest increase in $\delta^{18}\text{O}_p$ of 0.5‰ (figure 9 and table 3). Simulations with a winter sea ice
435 reduction between 12% and 28% best fit the $\delta^{18}\text{O}$ anomaly of 2.5‰ observed at this location
436 (considering the $\pm 1\sigma$ uncertainty on the best fit curve - figure 10e).



437

438 **Figure 10.** Simulated $\delta^{18}\text{O}$ anomalies as a function of winter (March) sea ice retreat. Ice core sites
 439 shown: (a) NEEM, (b) NGRIP, (c) GRIP, (d) Renland, (e) Camp Century, (f) DYE3, (g) GISP2. The
 440 retreat of sea ice is calculated as the percentage change in winter (March) sea ice extent compared
 441 to the PI experiment. Results for each of the 21 sea ice sensitivity experiments are represented by
 442 triangles. Solid lines signify best fit lines (fit = $b * (\log(x) - a)$). Also shown $\pm 1\sigma$ (lines with dashes)
 443 and $\pm 3\sigma$ uncertainty (shade envelopes) on the best fit curve. The observed $\delta^{18}\text{O}$ anomalies at each
 444 ice core site are marked with a black horizontal line with dashes. Black vertical lines with dashes
 445 represent the intersections with best fit line and $\pm 1\sigma$ uncertainty lines.

	NEEM	NGRIP	GRIP	Renland	Camp Century	DYE3	GISP2
	Observed $\delta^{18}\text{O}$ anomalies (‰)						
	3.6	3.1	3.5	3.5	2.5	4.7	2.7
Exp ID	Modelled $\delta^{18}\text{O}$ anomalies (‰)						
125-ka control	1.7	1.4	1.1	0.2	0.5	-0.3	1.1
WSIR-7	2.6	2.2	1.6	0.6	1.6	-0.1	1.6
WSIR-35	3.6	3.2	2.8	1.8	3.6	0.9	2.8
WSIR-94	3.7	3.2	2.7	1.4	3.7	1.1	2.7

446 **Table 3.** Modelled annual mean precipitation-weighted $\delta^{18}\text{O}$ anomalies (‰) at seven ice core sites
447 (NEEM, NGRIP, GRIP, Renland Camp Century, DYE3 and GISP2) for selected LIG simulations.
448 Also shown $\delta^{18}\text{O}$ anomalies observed in LIG ice relative to present day values reported by NEEM
449 community members, (2013) and Johnsen and Vinther (2007).

450 At GRIP, Renland and DYE3 sites, LIG $\delta^{18}\text{O}$ values were determined to be 3.5‰, 3.5‰, and
451 4.7‰ higher than present day values respectively (Johnsen and Vinther 2007). Depending on
452 the sea ice forcing, simulated $\delta^{18}\text{O}_p$ anomalies vary between 1.6‰ and 3.0‰ at GRIP, between
453 0.6‰ and 1.9‰ at Renland and between -0.1‰ and 1.1‰ at DYE3 (figure 9 and table 3).
454 Thus, none of our LIG sea ice sensitivity experiments are able to capture the strong $\delta^{18}\text{O}$
455 enrichment reported at these three locations. The underestimated anomalies may be explained
456 by the missing GIS elevation changes in the model runs, or other boundary condition changes
457 not implemented in our simulations, or the uncertainty on both modelled $\delta^{18}\text{O}$ values (see
458 appendix B) and ice core measurements. This will be discussed in more detail in section 4.

459 **4. Discussion**

460 **4.1. Estimating the Arctic LIG sea ice retreat from Greenland ice core $\delta^{18}\text{O}$**

461 Loss of NH sea ice, alongside increased Arctic SSTs, enhances evaporation over the Arctic
462 Ocean and consequently enriches $\delta^{18}\text{O}$ values over Greenland. This is a result of isotopically
463 heavy water vapour and a shorter distillation path between the Arctic and Greenland. Thus, in
464 line with previous studies, we have also confirmed that variations in sea ice and sea surface
465 conditions lead to polar impacts on $\delta^{18}\text{O}$ (Holloway et al., 2016a; Sime et al., 2013; Sjolte et
466 al., 2014). However, all ice core sites indicate that Greenland $\delta^{18}\text{O}$ has a lower sea ice
467 sensitivity as the LIG winter sea ice loss becomes greater than 40-50% (figure 10). This

468 behavior is very likely to be related to the higher sensitivity of Greenland $\delta^{18}\text{O}$ to GIS proximal
469 sea ice. Thus when the winter sea ice proximal to Greenland has been lost, $\delta^{18}\text{O}$ in Greenland
470 has almost no sensitivity to further sea ice loss. For this reason, whilst Greenland core data
471 allows determination of sea ice change near Greenland, it may not allow insight into the
472 possibility of near complete Arctic LIG sea ice loss.

473 The seven ice core records, which contain LIG ice, all indicate an increase in $\delta^{18}\text{O}$ across
474 Greenland between the present and LIG (Johnsen and Vinther 2007; NEEM community
475 members, 2013). HadCM3 simulations with greater than a 14%, 17% and 16% reduction in
476 winter sea ice extent (compared to the PI simulation) best fit the NGRIP, NEEM and GISP2
477 LIG $\delta^{18}\text{O}$ ice core data. For Camp Century core site, a winter sea ice reduction between 12%
478 and 28% best fits the observed $\delta^{18}\text{O}$ anomaly. Our HadCM3 simulations of the response to sea
479 ice retreat undershoot the recorded $\delta^{18}\text{O}$ anomalies at Renland, DYE3 and GRIP. Thus we
480 cannot simulate the LIG ice core $\delta^{18}\text{O}$ at these sites solely via a forced retreat of Arctic sea ice:
481 the model used here may not be adequately capturing the features at Renland due to its coarse
482 spatial resolution, and relatively tiny size of the coastal Renland icecap. Although, that said,
483 the summertime sea ice pack is too small in the PI simulation; a larger PI summer sea ice pack
484 would increase the potential size of the LIG $\delta^{18}\text{O}$ anomaly, likely somewhat improving the
485 model-data match at Renland, DYE3, and GRIP.

486 The existing observations of LIG Arctic sea ice cover are sparse and not quantitative.
487 Moreover, there is not a current consensus on the presence of perennial (Stein et al., 2017) or
488 seasonal sea ice cover (e.g. Adler et al. 2009; Brigham-Grette and Hopkins, 1995; Spielhagen
489 et al., 2004) over the central LIG Arctic Ocean in the marine core literature. Thus going beyond
490 a qualitative agreement on sea ice retreat between our LIG sea ice results and current marine
491 data is difficult. Additional marine core data, which helps establish the maximum extent of the

492 LIG sea ice retreat, would be particularly valuable to further evaluate our quantitative sea ice
493 retreat reconstruction.

494 **4.2. What caused this LIG Arctic sea ice retreat?**

495 Proxy data indicate that it is likely that in contrast to present day, there was both reduced winter
496 and summer sea ice extent during the LIG (e.g. Brigham-Grette and Hopkins, 1995; Stein et
497 al., 2017). However, our 125 ka control simulation, forced by GHG and orbital changes,
498 actually shows a 3% increase in winter sea ice and only a rather tiny reduction in the summer
499 sea ice. Many GCMs also have difficulty in accurately capture recent changes in the Arctic sea
500 ice that has occurred during the past decades (e.g. Stroeve et al., 2007, 2012). Thus factors
501 behind the inaccurate representation of historical sea ice variations by GCMs could indicate
502 deficiencies in model physics, for example in the simulation of ocean circulation and heat
503 changes, and/or possible over-simplifications of sea ice model physics e.g. schemes of sea-ice
504 albedo parameterization (e.g. Stroeve et al., 2012). These issues can all affect the simulation of
505 sea ice loss (or increase). However, that said, we believe it is more likely that the LIG retreat
506 of Arctic sea ice was caused by long term changes in meltwater influences over the course of
507 Termination 2 (T2) and the LIG, and subsequent changes of oceanic heat flows into the North
508 Atlantic and Arctic (Capron et al., 2014; Stone et al., 2016).

509 Capron et al (2014) demonstrate that meltwater from the NH deglaciation likely cooled the
510 Atlantic early in the LIG, enabling better simulation of LIG marine core SST data. A possible
511 subsequent build-up of heat, that was a likely consequence of this early LIG NH meltwater
512 (Capron et al., 2014; Stone et al., 2016), in the rest of the global ocean, and later advection of
513 excess heat to the North Atlantic could then have created the conditions that gave rise of the
514 retreat of 125 ka LIG sea ice. However few, if any, sufficiently long GCM simulations with
515 NH meltwater have been attempted for the LIG. In addition to a lack meltwater forcing, and

516 sufficient duration simulations, there may also be a lack of possible other relevant forcing
517 changes, for example changes in the Bering Strait flow during T2.

518 **4.3. Uncertainties on LIG $\delta^{18}\text{O}$ from Greenland ice cores**

519 The sea ice retreat insights provided from our study are dependent on the uncertainties attached
520 to Greenland LIG $\delta^{18}\text{O}$ ice core data. Except for the analytical uncertainty (of around 0.1‰),
521 it is indeed not straightforward how to quantify the additional uncertainties that originate
522 from the dating of the LIG layers, the possibility of missing LIG layers and also the lack of
523 constraints on elevation changes at some sites, especially DYE3.

524 NEEM is the only Greenland ice core where the disturbed bottom ice has been dated with good
525 accuracy. This huge achievement enabled recovery of the first well-dated Greenland LIG
526 record which covered the whole period from 114.5 to 128.5 ka (NEEM community members,
527 2013). Absolute dating uncertainties on this record are estimated to be around 2000 years
528 (Govin et al., 2015). For the LIG ice at the bottom of other Greenland cores, the dating
529 uncertainties are probably significantly larger. While tentative reconstructions of the
530 chronology of the bottom of the GRIP and GISP2 ice cores have been made using gas record
531 synchronization with Antarctic ice cores (Landais et al, 2003, Suwa et al. 2006), dating the
532 bottom of DYE3 and Camp Century is limited due to the poor preservation of the deep samples.
533 In contrast, the bottom ice stratigraphy at NGRIP is undisturbed so ice dating is much more
534 certain. However for NGRIP, the removal of an older LIG section by basal melt has left a lack
535 of data available to inform glaciological flow modelling used to establish the age model
536 (NGRIP members, 2004), thus again even with this undisturbed ice, the age of the bottom ice
537 is not known any better than 2000 years.

538 In addition to the dating uncertainties, ice flow can significantly affect ice core $\delta^{18}\text{O}$. At some
539 sites the bottom ice has flowed down to the drill site from higher elevation. Thus elevation

540 change between deposition site and drill site adds to the uncertainty of the observed differences
541 between LIG to present day $\delta^{18}\text{O}$. Based on total air content analysis it is, believed however
542 that central Greenland elevation was likely unchanged during the LIG (Raynaud et al. 1997),
543 and the Renland LIG ice also very likely originated from elevations very close to present
544 (Johnsen and Vinther 2007).

545 **4.4. Ice sheet, temperature, and wider atmospheric circulation changes**

546 This study focusses on examining the $\delta^{18}\text{O}$ signal of Arctic sea ice changes across Greenland,
547 and does not simulate any ice sheet changes, or attempt to reconstruct temperature changes at
548 ice core sites. Nevertheless, we make some comments on GIS, temperature, and wider
549 atmospheric circulation LIG changes.

550 It has been postulated that the GIS experienced significant change in volume and morphology
551 between the present and LIG (e.g. Church et al., 2013; Dutton et al., 2015). Thus, in addition
552 to sea ice effects, LIG $\delta^{18}\text{O}$ signals in Greenland ice cores may also be influenced by changes
553 in the GIS topography. GIS elevation changes would have also affected temperature at ice core
554 sites since lapse rate effects must have occurred, alongside atmospheric circulation and
555 precipitation changes (Merz et al., 2014b). Since most previous studies have suggested that the
556 LIG GIS was smaller than present (e.g. Church et al., 2013; Dutton et al., 2015), this also
557 suggests that larger LIG temperature rises occurred at ice core sites than shown in our
558 simulations, which feature no GIS change.

559 Previous modelling studies (e.g. Merz et al. 2016; Pederson et al. 2016b; Lunt et al., 2013), all
560 show a smaller warming at NEEM compared to the published values of $8\pm 4^\circ\text{C}$ warming (based
561 on $\delta^{18}\text{O}$ data - NEEM community members, 2013) and $8\pm 2.5^\circ\text{C}$ warming (based on $\delta^{15}\text{N}$ data
562 - Landais et al., 2016). Our medium sea ice loss (WSIR-35) simulation shows a warming of
563 3.5°C at the NEEM deposition site. If an additional moderate reduction of NEEM's surface

564 elevation, of 130±300m lower than present (as proposed by the NEEM community members,
565 2013), were incorporated, an extra warming of around 1.3-4.3°C (assuming an approximate
566 lapse rate of 1°C warmer per 100m height decrease) would occur. This would lead to a possible
567 core site warming of between 4.8°C and 7.8°C.

568 Note also that the sea ice loss simulations (including WSIR-35) probably underestimate NEEM
569 warming due to 125 ka sea surface condition changes. This is because the simulations exhibit
570 somewhat less Northern Atlantic warming than would be expected due to our method of forcing
571 the model to lose sea ice. Thus further studies examining the joint impacts of GIS change and
572 sea ice change on Greenland, alongside long meltwater influence simulations, would all be
573 most helpful in aiding a better understanding of what drove the LIG Greenland warming.

574 In terms of atmospheric circulation changes over the wider North Atlantic region, it is also
575 worth noting that sea ice loss and increased temperatures induce a significant drop in MSLP
576 that extends well into the North Pacific. These variations also modify precipitation patterns
577 over the whole Arctic region.

578 **5. Conclusions**

579 In conclusion, this study is a useful complement to previous LIG modelling studies. It
580 highlights the importance of understanding the impact of NH sea ice changes on the LIG
581 Greenland isotopic maximum. Our results show, for the first time, that variations in NH sea ice
582 conditions can lead to substantial LIG Greenland $\delta^{18}\text{O}$ increases which are commensurate with
583 $\delta^{18}\text{O}$ anomalies observed at NEEM, NGRIP, GISP2 and Camp Century sites. Further modelling
584 studies looking at the combined impact of a smaller GIS and NH sea ice variations, together
585 with additional LIG Arctic sea ice proxies, may help in understanding outstanding model-data
586 mismatches and in evaluating whether Arctic sea ice retreat is indeed a major factor responsible
587 for the high LIG $\delta^{18}\text{O}$ measured in Greenland ice cores.

588 **Acknowledgments**

589 We thank Kira Rehfeld for constructive discussion and Peter Hopcroft for his advice on sea ice
590 forcing. We thank the two reviewers for their constructive comments, which helped improved
591 the manuscript through the review process. IMV acknowledges a NERC GW4+ studentship
592 and support provided through the EPSRC-funded Past Earth Network (Grant number
593 EP/M008363/1). LCS acknowledges additional support provided through grants
594 NE/P009271/1, NE/P013279/1, and NE/J004804/1. EC is funded by the European Union's
595 Seventh Framework Programme for research and innovation under the Marie Skłodowska-
596 Curie grant agreement no 600207. BV has received funding from the European Research
597 Council under the European Community's Seventh Framework Programme (FP7/2007-2013) /
598 ERC grant agreement 610055 as part of the ice2ice project.

599 **Data availability**

600 Access to the Met Office Unified Model source code is available under licence from the Met
601 Office at <https://www.metoffice.gov.uk/research/collaboration/um-partnership>. The climate
602 model data are available on request from <http://www.bridge.bris.ac.uk/resources/simulations>.

603 **References**

- 636 Adler, R.E., Polyak, L., Ortiz, J.D., Kaufman, D.S., Channell, J.E.T., Xuan, C., Grottole, A.G.,
637 Selln, E., Crawford, K.A., 2009. Sediment record from the western Arctic Ocean with an
638 improved Late Quaternary age resolution: HOTRAX core HLY0503-8JPC, Mendeleev
639 Ridge. *Global and Planetary Change* 68, 18-29.
640 <https://doi.org/10.1016/j.gloplacha.2009.03.026>.
- 641 Bauch, H.A., and Erlenkeuser, H., 2008. A “critical” climatic evaluation of last interglacial
642 (MIS 5e) records from the Norwegian Sea. *Polar Res.* 27, 135-151.
643 <https://doi.org/10.1111/j.1751-8369.2008.00059.x>.
- 644 Bauch, H.A., Kandiano, E.S., Helmke, J.P., 2012. Contrasting ocean changes between the
645 subpolar and polar North Atlantic during the past 135 ka. *Geophys. Res. Lett.*, 39, L11604.
646 <https://doi.org/10.1029/2012GL051800>.
- 647 Brigham-Grette, J., and Hopkins, D.M., 1995. Emergent-marine record and paleoclimate of the
648 last interglaciation along the northwest Alaskan coast. *Quat. Res.* 43, 159-173.
649 <https://doi.org/10.1006/qres.1995.1017>.
- 650 Brigham-Grette, J., Hopkins, D.M., Ivanov, V.F., Basilyan, A., Benson, S.L., Heiser, P.,
651 Pushkar, V., 2001. Last interglacial (Isotope stage 5) glacial and sea level history of coastal
652 Chukotka Peninsula and St. Lawrence Island, western Beringia. *Quat. Sci. Rev.* 20, 419-
653 436. [https://doi.org/10.1016/S0277-3791\(00\)00107-4](https://doi.org/10.1016/S0277-3791(00)00107-4).
- 654 CAPE Last Interglacial Project members, 2006. Last Interglacial Arctic warmth confirms polar
655 amplification of climate change. *Quat. Sci. Rev.* 25, 1383-1400.
656 <https://doi.org/10.1016/j.quascirev.2006.01.033>.
- 657 Capron, E., Govin, A., Stone, E. J., Masson-Delmotte, V., Mulitza, S., Otto-Bliesner, B.,
658 Rasmussen, T. L., Sime, L. C., Waelbroeck, C., Wolff, E., 2014. Temporal and spatial
659 structure of multi-millennial temperature changes at high latitudes during the Last
660 Interglacial. *Quat. Sci. Rev.* 103, 116-133. <https://doi.org/10.1016/j.quascirev.2014.08.018>.
- 661 Capron, E., Govin, A., Feng, R., Otto-Bliesner, B.L., Wolff, E.W., 2017. Critical evaluation of
662 climate syntheses to benchmark CMIP6/PMIP4 127 ka Last Interglacial simulations in the
663 high-latitude regions. *Quat. Sci. Rev.* 168, 137-150.
664 <https://doi.org/10.1016/j.quascirev.2017.04.019>.
- 665 Church, J.A., Clark, P.U., Cazenave, A., Gregory, J.M., Jevrejeva, S., Levermann, A.,
666 Merrifield, M.A., Milne, G.A., Nerem, R.S., and Nunn, P.D., Payne, A.J., Pfeffer, W.T.,
667 Stammer, D., Unnikrishnan, A.S., 2013. Sea level change in *Climate Change 2013: The*
668 *Physical Science Basis, Contribution of Working Group I to the Fifth Assessment Report of*
669 *the Intergovernmental Panel on Climate Change*. [Stocker, T.F., D. Qin, G.-K. Plattner, M.
670 Tignor, S.K. Allen, J. Boschung, A. Nauels, Y. Xia, V. Bex and P.M. Midgley (eds.)].
671 Cambridge University Press, Cambridge, United Kingdom and New York, NY, USA, 1137-
672 1216.
- 673 Cronin, T.M., Gemery, L., Briggs Jr., W.M., Jakobsson, M., Polyak, L., Brouwers, E.M., 2010.
674 Quaternary Sea-ice history in the Arctic Ocean based on a new Ostracode sea-ice proxy.
675 *Quat. Sci. Rev.* 29, 3415-3429. <https://doi.org/10.1016/j.quascirev.2010.05.024>.
- 676 Dansgaard, W., 1964. Stable isotopes in precipitation. *Tellus* 16, 436-468.

677 Dansgaard, W., Johnsen S.J., Moller, J., Langway, C.C., 1969. One thousand centuries of
678 climatic record from Camp Century on the Greenland ice sheet. *Science*, 166, 377-381.
679 <https://doi.org/10.1126/science.166.3903.377>.

680 Dansgaard, W., Clausen, H. B., Gundestrup, N., Hammer, C. U., Johnsen, S. J., Kristinsdottir,
681 M., Reeh, N., 1982. A New Greenland Deep Ice Core. *Science*, 218, 1273-1277.
682 <https://doi.org/10.1126/science.218.4579.1273>.

683 Dutton, A., Carlson, A. E., Long, A. J., Milne, G. A., Clark, P. U., DeConto, R., Horton, B. P.,
684 Rahmstorf, S., Raymo, M. E., 2015. Sea-level rise due to polar ice-sheet mass loss during
685 past warm periods. *Science*, 349, 6244. <https://doi.org/10.1126/science.aaa4019>.

686 Gierz, P., Werner, M., Lohmann, G., 2017. Simulating climate and stable water isotopes during
687 the Last Interglacial using a coupled climate-isotope model. *J. Adv. Model. Earth Syst.*, 9,
688 2027-2045. <https://doi.org/10.1002/2017MS001056>

689 Gordon, C., Cooper, C., Senior, C. A., Banks, H., Gregory, J. M., Johns, T. C., Mitchell, J. F.
690 B., Wood, R. A., 2000. The simulation of SST, sea ice extents and ocean heat transports in
691 a version of the Hadley Centre coupled model without flux adjustments. *Clim. Dynam.*, 16,
692 147-168. <https://doi.org/10.1007/s003820050010>.

693 Govin, A., Braconnot, P., Capron, E., Cortijo, E., Duplessy, J.-C., Jansen, E., Labeyrie, L.,
694 Landais, A., Marti, O., Michel, E., Mosquet, E., Risebrobakken, B., Swingedouw, D., and
695 Waelbroeck, C., 2012. Persistent influence of ice sheet melting on high northern latitude
696 climate during the early Last Interglacial. *Clim. Past* 8, 483-507. [https://doi.org/10.5194/cp-](https://doi.org/10.5194/cp-8-483-2012)
697 [8-483-2012](https://doi.org/10.5194/cp-8-483-2012).

698 Govin, A., Capron, E., Tzedakis, P.C., Verheyden, S., Ghaleb, B., Hillaire-Marcel, C., St-Onge,
699 G., Stoner, J.S., Bassinot, F., Bazin, L., Blunier, T., Combourieu-Nebout, N., El Ouahabi,
700 A., Genty, D., Gersonde, R., Jimenez-Amat, P., Landais, A., Martrat, B., Masson-Delmotte,
701 V., Parrenin, F., Seidenkrantz, M.-S., Veres, D., Waelbroeck, C., Zahn, R., 2015. Sequence
702 of events from the onset to the demise of the Last Interglacial: Evaluating strengths and
703 limitations of chronologies used in climatic archives. *Quat. Sci. Rev.* 129, 1-36.
704 <https://doi.org/10.1016/j.quascirev.2015.09.018>.

705 GRIP members, 1993. Climate instability during the last interglacial period recorded in the
706 GRIP ice core. *Nature*, 364, 203-207. <https://doi.org/10.1038/364203a0>.

707 Grootes, P. M., Stuiver, M., White, J. W. C., Johnsen, S. J., Jouzel, J., 1993. Comparison of
708 oxygen isotope records from the GISP2 and GRIP Greenland ice cores. *Nature*, 366, 552–
709 554. <https://doi.org/doi:10.1038/366552a0>.

710 Hoffman, J.S., Clark, P.U., Parnell, A.C., He, F., 2017. Regional and global sea-surface
711 temperatures during the last interglaciation. *Science* 355, 276-279.
712 <https://doi.org/10.1126/science.aai8464>.

713 Holloway, M.D., Sime, L.C., Singarayer, J.S., Tindall, J.C., Bunch, P., Valdes, P.J., 2016a.
714 Antarctic last interglacial isotope peak in response to sea ice retreat not ice-sheet collapse.
715 *Nature communications*, 7, 12293. <https://doi.org/10.1038/ncomms12293>.

716 Holloway, M.D., Sime, L.C., Singarayer, J.S., Tindall, J.C., Valdes, P.J., 2016b.
717 Reconstructing paleosalinity from $\delta^{18}\text{O}$: Coupled model simulations of the Last Glacial
718 Maximum, Last Interglacial and Late Holocene. *Quat. Sci. Rev.*, 131, 350-364.
719 <https://doi.org/10.1016/j.quascirev.2015.07.007>.

720 Holloway, M.D., Sime, L.C., Allen, C.S., Hillenbrand, C., Bunch, P., Wolff, E., Valdes, P.J.,
721 2017. The spatial structure of the 128 ka Antarctic sea ice minimum. *Geophys. Res. Lett.*,
722 44, 11129–11139. <https://doi.org/10.1002/2017GL074594>.

723 Howell, F.W., Haywood, A.M., Dolan, A.M., Dowsett, H.J., Francis, J.E., Hill, D.J.,
724 Pickering, S.J., Pope, J.O., Salzmann, U. Wade, B.S., 2014. Can uncertainties in sea ice
725 albedo reconcile patterns of data-model discord for the Pliocene and 20th/21st centuries?
726 *Geophys. Res. Lett.*, 41, 2011-2018. <https://doi.org/10.1002/2013GL058872>.

727 IPCC, 2013. *Climate Change 2013: The Physical Science Basis. Contribution of Working*
728 *Group I to the Fifth Assessment Report of the Intergovernmental Panel on Climate Change*
729 [Stocker, T.F., D. Qin, G.-K. Plattner, M. Tignor, S.K. Allen, J. Boschung, A. Nauels, Y.
730 Xia, V. Bex and P.M. Midgley (eds.)]. Cambridge University Press, Cambridge, United
731 Kingdom and New York, NY, USA, 1535 pp.

732 Johnsen, S. J., Dahl-Jensen, D., Gundestrup, N., Steffensen, J. P., Clausen, H. B., Miller, H.,
733 Masson-Delmotte, V., Sveinbjörnsdóttir, A. E., White, J., 2001. Oxygen isotope and
734 palaeotemperature records from six Greenland ice-core stations: Camp Century, Dye-3,
735 GRIP, GISP2, Renland and NorthGRIP, *J. Quat. Sci.*, 16, 299-307.
736 <https://doi.org/10.1002/jqs.622>.

737 Johnsen, S. and Vinther, B. 2007. Ice core records – Greenland stable isotopes, in: Elias, S.A.,
738 (Eds), *Encyclopedia of Quaternary Science.*, Elsevier, Oxford, pp. 1250-1258.

739 Jones, C.P., 1995. Unified model documentation paper No 70. Specification of ancillary fields
740 by C P Jones. Version 4 dated 04/12/95.

741 Jouzel, J., Koster, R.D., Suozzo, R.J., Russell, G.L., 1994. Stable water isotope behaviour
742 during the last glacial maximum: a general circulation model analysis. *J. Geophys. Res.* 99,
743 25791-25801. <https://doi.org/10.1029/94JD01819>.

744 Jouzel, J., Alley, R.B., Cuffey, K.M., Dansgaard, W., Grootes, P., Hoffmann, G., Johnsen, S.J.,
745 Koster, R.D., Peel, D., Shuman, C., Stievenard, M., Stuiver, M., White, J., 1997. Validity
746 of the temperature reconstruction from water isotopes in ice cores. *J. Geophys. Res.* 102,
747 26471-26487. <https://doi.org/10.1029/97JC01283>.

748 Kopp, R.E., Simons, F.J., Mitrovica, J.X., Maloof, A.C., Oppenheimer, M., 2009. Probabilistic
749 assessment of sea level during the last interglacial stage. *Nature* 462, 863-867
750 <http://dx.doi.org/10.1038/nature08686>.

751 Langebroek, P.M., Nisancioglu, K.H., 2014. Simulating last interglacial climate with NorESM:
752 role of insolation and greenhouse gases in the timing of peak warmth. *Clim, Past*, 10, 1305-
753 1318. <http://dx.doi.org/10.5194/cp-10-1305-2014>.

754 Landais, A., Chappellaz, J., Delmotte, M., Jouzel, J., Blunier, T., Bourg, C., Caillon, N.,
755 Cherrier, S., Malaizé, B., Masson-Delmotte, V., Raynaud, D., Schwander, J., Steffensen,
756 J.P., 2003. A tentative reconstruction of the last interglacial and glacial inception in
757 Greenland based on new gas measurements in the Greenland Ice Core Project (GRIP) ice
758 core. *J. Geophys. Res.*, 108, D18, 4563. <https://doi.org/10.1029/2002JD003147>.

759 Landais, A., Masson-Delmotte, V., Capron, E., Langebroek, P. M., Bakker, P., Stone, E. J.,
760 Merz, N., Raible, C. C., Fischer, H., Orsi, A., Prié, F., Vinther, B., Dahl-Jensen, D., 2016.
761 How warm was Greenland during the last interglacial period? *Clim. Past*, 12, 1933-1948.
762 <http://dx.doi.org/10.5194/cp-12-1933-2016>.

763 Lunt, D. J., Abe-Ouchi, A., Bakker, P., Berger, A., Braconnot, P., Charbit, S., Fischer, N.,
764 Herold, N., Jungclaus, J. H., Khon, V. C., Krebs-Kanzow, U., Langebroek, P. M., Lohmann,
765 G., Nisancioglu, K. H., Otto-Bliesner, B. L., Park, W., Pfeiffer, M., Phipps, S. J., Prange,
766 M., Rachmayani, R., Renssen, H., Rosenbloom, N., Schneider, B., Stone, E. J., Takahashi,
767 K., Wei, W., Yin, Q., Zhang, Z. S., 2013. A multi-model assessment of last interglacial
768 temperatures, *Clim. Past*, 9, 699-717. <http://dx.doi.org/10.5194/cp-9-699-2013>.

769 Liu, X., and Battisti, D. S., 2015. The influence of orbital forcing of tropical insolation on the
770 climate and isotopic composition of precipitation in South America. *J. of Climate*, 28(12),
771 4841-4862. <https://doi.org/10.1175/JCLI-D-14-00639.1>

772 McKay, N. P., Overpeck, J. T., Otto-Bliesner, B. L., 2011. The role of ocean thermal expansion
773 in Last Interglacial sea level rise. *Geophys. Res. Lett.*, 38, L14605.
774 <http://dx.doi.org/10.1029/2011GL048280>.

775 Masson-Delmotte, V., Jouzel, J., Landais, A., Stievenard, M., Johnsen, S.J., White, J.W.C.,
776 Werner, M., Sveinbjornsdottir, A., Fuhrer, K., 2005. GRIP deuterium excess reveals rapid
777 and orbital-scale changes in Greenland moisture origin. *Science*. 309(5731), 118-121.
778 <http://dx.doi.org/10.1126/science.1108575>.

779 Masson-Delmotte, V., Braconnot, P., Hoffmann, G., Jouzel, J., Kageyama, M., Landais, A.,
780 Lejeune, Q., Risi, C., Sime, L. C., Sjolte, J., Swingedouw, D., Vinther, B. M., 2011.
781 Sensitivity of interglacial Greenland temperature and $\delta^{18}\text{O}$: ice core data, orbital and
782 increased CO_2 climate simulations. *Clim. Past*, 7, 1041-1059. [http://dx.doi.org/10.5194/cp-](http://dx.doi.org/10.5194/cp-7-1041-2011)
783 [7-1041-2011](http://dx.doi.org/10.5194/cp-7-1041-2011).

784 Masson-Delmotte, V., Schulz, M., Abe-Ouchi, A., Beer, J., Ganopolski, A., González Rouco,
785 J. F., Jansen, E., Lambeck, K., Luterbacher, J., Naish, T., Osborn, T., Otto-Bliesner, B.,
786 Quinn, T., Ramesh, R., Rojas, M., Shao, X., Timmermann, A., 2013. Information from
787 Paleoclimate Archives, in: *Climate Change 2013: The Physical Science Basis. Contribution*
788 *of Working Group I to the Fifth Assessment Report of the Intergovernmental Panel on*
789 *Climate Change*. [Stocker, T.F., D. Qin, G.-K. Plattner, M. Tignor, S.K. Allen, J. Boschung,
790 A. Nauels, Y. Xia, V. Bex and P.M. Midgley (eds.)]. Cambridge University Press,
791 Cambridge, United Kingdom and New York, NY, USA, 383-464.

792 Meier, W., F. Fetterer, M. Savoie, S. Mallory, R. Duerr, J. Stroeve. 2017. NOAA/NSIDC
793 Climate Data Record of Passive Microwave Sea Ice Concentration, Version 3. Goddard
794 Merged sea ice record from 1979 to 1989. Boulder, Colorado USA. NSIDC: National Snow
795 and Ice Data Center. <http://dx.doi.org/10.7265/N59P2ZTG>. 17/10/2017.

796 Merz, N., Born, A., Raible, C. C., Fischer, H., Stocker, T. F., 2014a. Dependence of Eemian
797 Greenland temperature reconstructions on the ice sheet topography, 2014. *Clim. Past*, 10,
798 1221-1238. <http://dx.doi.org/10.5194/cp-10-1221-2014>.

799 Merz, N., Gfeller, G., Born, A., Raible, C. C., Stocker, T. F., Fischer, H., 2014b. Influence of
800 ice sheet topography on Greenland precipitation during the Eemian interglacial. *J. Geophys.*
801 *Res.*, 119, 10749-10768. <http://dx.doi.org/10.1002/2014JD021940>.

802 Merz, N., Born, A., Raible, C. C., Stocker, T. F., 2016. Warm Greenland during the last
803 interglacial: the role of regional changes in sea ice cover. *Clim. Past*, 12, 2011–2031.
804 <https://doi.org/10.5194/cp-12-2011-2016>.

805 NEEM community members, 2013. Eemian interglacial reconstructed from a Greenland folded
806 ice core. *Nature*, 493, 489–494. <https://doi.org/10.1038/nature11789>.

807 NGRIP Project Members, 2004. High-resolution record of Northern Hemisphere climate
808 extending into the last interglacial period. *Nature* 431, 147-151.
809 <https://doi.org/10.1038/nature02805>.

810 Nørgaard-Pedersen, N., Mikkelsen, N., Lassen, S.J., Kristoffersen, Y., Sheldon, E., 2007.
811 Reduced sea ice concentrations in the Arctic Ocean during the last interglacial period
812 revealed by sediment cores off northern Greenland. *Paleoceanography* 22, PA1218.
813 <http://dx.doi.org/10.1029/2006PA001283>.

814 Otto-Bliesner, B.L., Marshall, S.J., Overpeck, J.T., Miller, G.H., Hu, A., CAPE Last
815 Interglacial Project members., 2006. Simulating arctic climate warmth and icefield retreat
816 in the Last Interglacial. *Science*, 311, 1751-1753.
817 <http://dx.doi.org/10.1126/science.1120808>.

818 Otto-Bliesner, B., Rosenbloom, N., Stone, E., McKay, N.P., Lunt, D.J., Brady, E.C., Overpeck,
819 J.T., 2013. How warm was the Last Interglacial? New model-data comparisons. *Philos.*
820 *Trans. R. Soc. A Phys. Math. Eng. Sci.*, 371. <http://dx.doi.org/10.1098/rsta.2013.0097>.

821 Pedersen, R.A., Langen, P.L., Vinther, B.M., 2016a. The last interglacial climate: comparing
822 direct and indirect impacts of insolation changes. *Clim. Dynam*, 48, 3391-3407.
823 <http://dx.doi.org/10.1007/s00382-016-3274-5>.

824 Pedersen, R.A., Langen, P.L., Vinther, B.M., 2016b. Greenland during the last interglacial: the
825 relative importance of insolation and oceanic changes. *Clim. Past*, 12, 1907-1918.
826 <http://dx.doi.org/10.5194/cp-12-1907-2016>.

827 Peng, G., Meier, W.N., Scott, D.J., Savoie, M.H., 2013. A long-term and reproducible passive
828 microwave sea ice concentration data record for climate studies and monitoring. *Earth Syst.*
829 *Sci. Data* 5. 311-318. <http://dx.doi.org/10.5194/essd-5-311-2013>.

830 Raynaud, D., Chappellaz, J., Ritz, C., Martinerie, P., 1997. Air content along the Greenland
831 Ice Core Project core: A record of surface climatic parameters and elevation in central
832 Greenland. *J. Geophys. Res.*, 102, C12, 26607-26613.

833 Rehfeld, K., Münch, T., Ho, S.L., Laepple, T., 2018. Global patterns of declining temperature
834 variability from the Last Glacial Maximum to the Holocene. *Nature*, 554, 356-359.
835 <http://dx.doi.org/10.1038/nature25454>.

836 Schmidt, G.A., LeGrande, A.N., Hoffmann, G., 2007. Water isotope expressions of intrinsic
837 and forced variability in a coupled ocean-atmosphere model. *J. Geophys. Res.*, 112,
838 D10103. <http://dx.doi.org/10.1029/2006JD007781>.

839 Schmidt, G.A., Annan, J.D., Bartlein, P.J., Cook, B.I., Guilyardi, E., Hargreaves, J.C.,
840 Harrison, S.P., Kageyama, M., LeGrande, A.N., Konecky, B., Lovejoy, S., Mann, M.E.,
841 Masson-Delmotte, V., Risi, C., Thompson, D., Timmermann, A., Tremblay, L.B., Yiou, P.,
842 2014. Using palaeo-climate comparisons to constrain future projections in CMIP5. *Clim.*
843 *Past*, 10, 221-250. <http://dx.doi.org/10.5194/cp-10-221-2014>.

844 Sime, L. C., Risi, C., Tindall, J. C., Sjolte, J., Wolff, E. W., Masson-Delmotte, V., Capron, E.,
845 2013. Warm climate isotopic simulations: what do we learn about interglacial signals in
846 Greenland ice cores? *Quat. Sci. Rev.* 67, 59-80.
847 <https://doi.org/10.1016/j.quascirev.2013.01.009>.

848 Sjolte, J., Hofmann, G., Johnsen, S.J., 2014. Modelling the response of stable water isotopes in
849 Greenland precipitation to orbital configurations of the previous interglacial. *Tellus B:*
850 *Chemical and Physical Meteorology*, 66, 22872. <https://doi.org/10.3402/tellusb.v66.22872>

851 Spielhagen, R. F., Baumann, K., Erlenkeuser, H., Nowaczyk, N. R., Nørgaard-Pedersen, N.,
852 Vogt, C., Weiel, D., 2004. Arctic Ocean deep-sea record of Northern Eurasian ice sheet
853 history. *Quat. Sci. Rev.* 23, 1455-1483. <https://doi.org/10.1016/j.quascirev.2003.12.015>.

854 Steffensen, J. P., Andersen, K. K., Bigler, M., Clausen, H. B., Dahl-Jensen, D. and co-authors,
855 2008. High-resolution Greenland ice core data show abrupt climate change happens in few
856 years. *Science*. 321(5889), 680-684. <https://doi.org/10.1126/science.1157707>.

857 Steig, E. J., Grootes, P. M., Stuiver, M., 1994. Seasonal Precipitation Timing and Ice Core
858 Records. *Science*, 266, 1885-1886. <https://doi.org/10.1126/science.266.5192.1885>.

859 Stein, R., Fahl, K., Gierz, P., Niessen, F., Lohmann., G., 2017. Arctic Ocean sea ice cover
860 during the penultimate glacial and the last interglacial. *Nature communications*, 8, 373.
861 <https://doi.org/10.1038/s41467-017-00552-1>.

862 Stone, E.J., Capron, E., Lunt, D.J., Payne, A.J., Singarayer, J.S., Valdes, P.J., Wolff, E.W.,
863 2016. Impact of meltwater on high-latitude early Last Interglacial climate. *Clim. Past*, 12,
864 1919-1932.

865 Stroeve, J., Holland, M.M., Meier, W., Scambos, T., Serreze, M., 2007. Arctic sea ice decline:
866 Faster than forecast, *Geophys. Res. Lett.*, 34, L09501.
867 <https://doi.org/10.1029/2007GL029703>.

868 Stroeve, J.C., Kattsov, V., Barrett, A., Serreze, M., Pavlova, T., Holland, M., Meier, W.N.,
869 2012. Trends in Arctic sea ice extent from CMIP5, CMIP3 and observations, *Geophys. Res.*
870 *Lett.*, 39, L16502. <https://doi.org/10.1029/2012GL052676>.

871 Suwa, M., von Fischer, J.C., Bender, M.L., Landais, A., Brook, E.J., 2006. Chronology
872 reconstruction for the disturbed bottom section of the GISP2 and the GRIP ice cores:
873 Implications for Termination II in Greenland. *J. of Geophys. Res.*, 111, D02101,
874 <https://doi.org/10.1029/2005JD006032>.

875 Tindall, J. C., Valdes, P. J. Sime, L. C., 2009. Stable water isotopes in HadCM3: Isotopic
876 signature of El Niño-Southern Oscillation and the tropical amount effect. *J. Geophys. Res.*
877 114, D04111. <https://doi.org/10.1029/2008JD010825>.

878 Tindall, J. C, Flecker, R., Valdes, P.J., Schimidt, D.N., Markwick, P., Harris, J., 2010.
879 Modelling the oxygen isotope distribution of ancient seawater using a coupled ocean-
880 atmosphere GCM: Implications for reconstructing early Eocene climate. *Earth Planet Sci.*
881 *Lett.* 292, 265-273. <https://doi.org/10.1016/j.epsl.2009.12.049>.

882 Tindall, J. C., and Haywood, A.L., 2015. Modeling oxygen isotopes in the Pliocene: Large-
883 scale features over the land and ocean. *Paleoceanography*, 30, 1183-1201.
884 <http://dx.doi.org/10.1002/2014PA002774>.

889 Turney, C.S.M., and Jones, R.T., 2010. Does the Agulhas Current amplify global temperatures
890 during super-interglacials? *J. Quat. Sci.*, 25 (6), 839-843.
891 <http://dx.doi.org/10.1002/jqs.1423>.

892 Vaughan, D. G., Comiso, J. C., Allison, I., Carrasco, J., Kaser, G., Kwok, R., Mote, P., Murray,
893 T., Paul, F., Ren, J., Rignot, E., Solomina, O., Steffen, K., and Zhang, T., 2013.
894 Observations: Cryosphere, in: *Climate Change 2013: The Physical Science Basis*,
895 Contribution of Working Group I to the Fifth Assessment Report of the Intergovernmental
896 Panel on Climate Change. [Stocker, T.F., D. Qin, G.-K. Plattner, M. Tignor, S.K. Allen, J.
897 Boschung, A. Nauels, Y. Xia, V. Bex and P.M. Midgley (eds.)]. Cambridge University
898 Press, Cambridge, United Kingdom and New York, NY, USA, 317-382.

899 Vinther, B. M., Buchardt, S. L., Clausen, H. B., Dahl-Jensen, D., Johnsen, S. J., Fisher, D.A.,
900 Koerner, R.M., Raynaud, D., Lipenkov, V., Andersen, K.K., Blunier, T., Rasmussen, S.O.,
901 Steffensen, J.P., Svensson, A.M. 2009. Holocene thinning of the Greenland ice sheet.
902 Nature, 461, 385-388. <https://doi.org/10.1038/nature08355>.

903 von Storch, H. and Zwiers, F. W., 2001. Statistical Analysis in Climate Research, Cambridge
904 University Press, Cambridge, UK and New York, NY, USA, 111-118 pp.

905 Werner, M., Langebroek, P.M., Carlsen, T., Herold, M., Lohmann, G., 2011. Stable water
906 isotopes in the ECHAM5 general circulation model: toward high-resolution isotope
907 modeling on a global scale. Journal of Geophysical Research 116, D15109.
908 <https://doi.org/doi:10.1029/2011JD015681>.

909

919 **Table 1.** Compilation of observations of NH sea ice changes for the LIG.

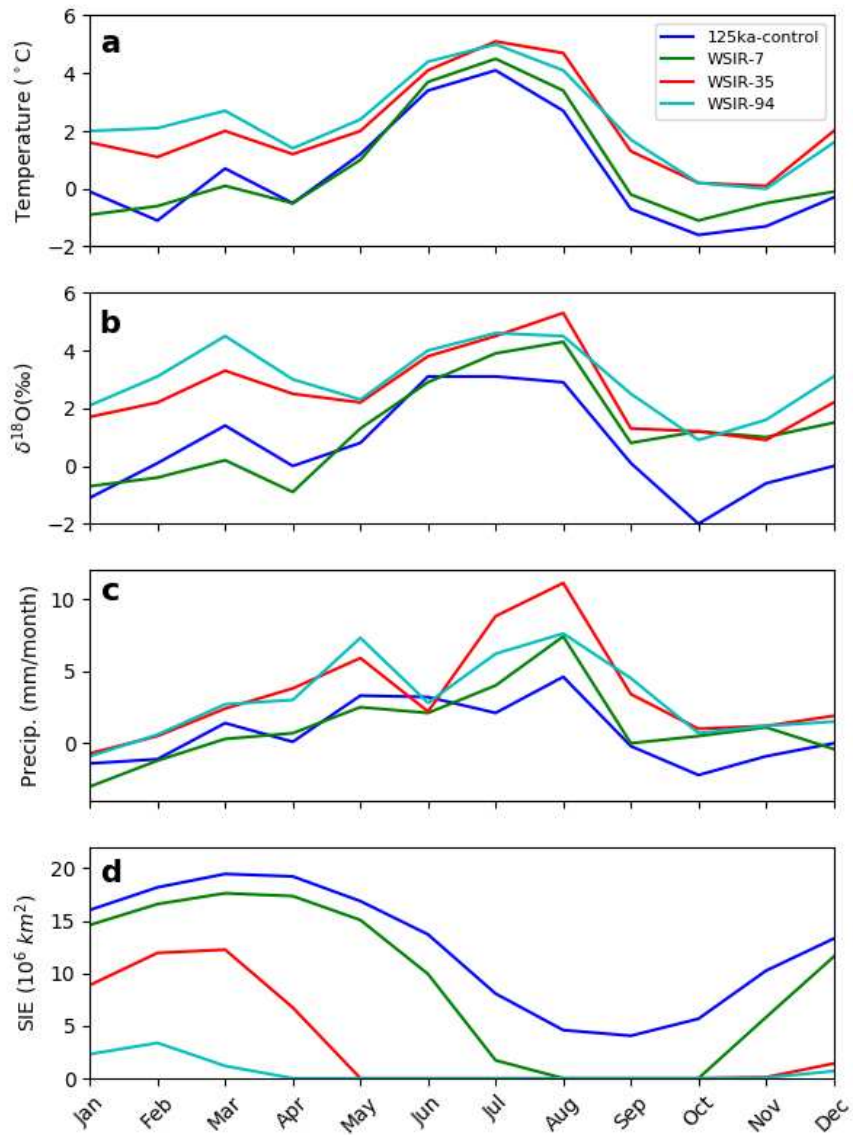
Site	Proxy	Comments	Reference
GreenICE (core 11)	Subpolar foraminifers	The presence of subpolar planktonic foraminifers in MIS 5e zone interpreted to indicate reduced sea ice cover compared to present.	Nørgaard-Pedersen et al., 2007
HLY0503-8JPC	Subpolar foraminifers	Subpolar planktonic foraminifers found in MIS 5e zone suggest reduced sea-ice cover, perhaps seasonally ice-free conditions.	Adler et al., 2009
Nome, St. Lawrence Island and Beaufort Sea shelf	Mollusc and ostracode faunas	Fossil assemblages suggest that the winter sea-ice limit did not expand south of Bering Strait, that the Bering Sea was annually ice-free and that the sea ice cover in the Arctic ocean was not perennial for some period.	Brigham-Grette and Hopkins. (1995)
NP26-5/32	Ostracode faunas	Ostracode <i>Acetabulastoma arcticum</i> , which inhabits exclusively in areas of perennial Arctic sea ice, occurs during late MIS 5e but it is absent during peak interglacial.	Cronin et al., (2010)
Oden96/12-1pc	Ostracode faunas	Ostracode <i>Acetabulastoma arcticum</i> , which inhabits exclusively in areas of perennial Arctic sea ice, occurs during late MIS 5e but it is absent during peak interglacial.	Cronin et al., (2010)
PS2200-5	Ostracode faunas	Ostracode <i>Acetabulastoma arcticum</i> , which inhabits exclusively in areas of perennial Arctic sea ice, occurs during late MIS 5e but it is absent during peak interglacial.	Cronin et al., (2010)
	Biomarker proxy IP25, terrestrial biomarkers and open-water phytoplankton biomarkers	Biomarker proxies suggest perennial sea ice cover in the central part of Arctic Ocean during MIS 5e.	Stein et al. (2017)
PS51/038-3	Biomarker proxy IP25, terrestrial biomarkers and open-water phytoplankton biomarkers	Biomarker proxies suggest perennial sea ice cover in the central part of Arctic Ocean during MIS 5e.	Stein et al. (2017)
PS2138-2	Biomarker proxy IP25, terrestrial biomarkers and open-water phytoplankton biomarkers	Biomarker proxies suggest seasonal open-water conditions over the Barents Sea continental margin.	Stein et al. (2017)

PS2757-8	Biomarker proxy IP25, terrestrial biomarkers and open-water phytoplankton biomarkers	Biomarker proxies suggest relatively closed sea ice cover conditions during MIS 5e.	Stein et al. (2017)
-----------------	---	---	------------------------

920 **Table 2.** Full list of simulations. The experiments marked in red are the ones mainly discussed in the text.

Exp ID	Eccentricity	Obliquity (°)	Perihelion (day of yr)	Prescribed heat flux (W m ⁻²)	CO ₂ (ppmv)	CH ₄ (ppbv)	N ₂ O (ppbv)	Percentage change in March Arctic sea ice extent relative to PI simulation (%)
PI	0.0167	23.45	1.7	0	280	760	270	0
125ka-control	0.04001	23.80	201.3	0	276	640	263	+3
WSIR-7	0.04001	23.80	201.3	15	276	640	263	-7
WSIR-11	0.04001	23.80	201.3	20	276	640	263	-11
WSIR-10	0.04001	23.80	201.3	25	276	640	263	-10
WSIR-15	0.04001	23.80	201.3	30	276	640	263	-15
WSIR-17	0.04001	23.80	201.3	35	276	640	263	-17
WSIR-17b	0.04001	23.80	201.3	40	276	640	263	-17
WSIR-19	0.04001	23.80	201.3	50	276	640	263	-19
WSIR-21	0.04001	23.80	201.3	55	276	640	263	-21
WSIR-22	0.04001	23.80	201.3	60	276	640	263	-22
WSIR-26	0.04001	23.80	201.3	80	276	640	263	-26
WSIR-35	0.04001	23.80	201.3	100	276	640	263	-35
WSIR-41	0.04001	23.80	201.3	120	276	640	263	-41
WSIR-54	0.04001	23.80	201.3	140	276	640	263	-54
WSIR-65	0.04001	23.80	201.3	145	276	640	263	-65
WSIR-72	0.04001	23.80	201.3	150	276	640	263	-72
WSIR-78	0.04001	23.80	201.3	155	276	640	263	-78
WSIR-81	0.04001	23.80	201.3	160	276	640	263	-81
WSIR-89	0.04001	23.80	201.3	180	276	640	263	-89
WSIR-94	0.04001	23.80	201.3	200	276	640	263	-94
WSIR-99	0.04001	23.80	201.3	250	276	640	263	-99
WSIR-100	0.04001	23.80	201.3	300	276	640	263	-100

921



922

923

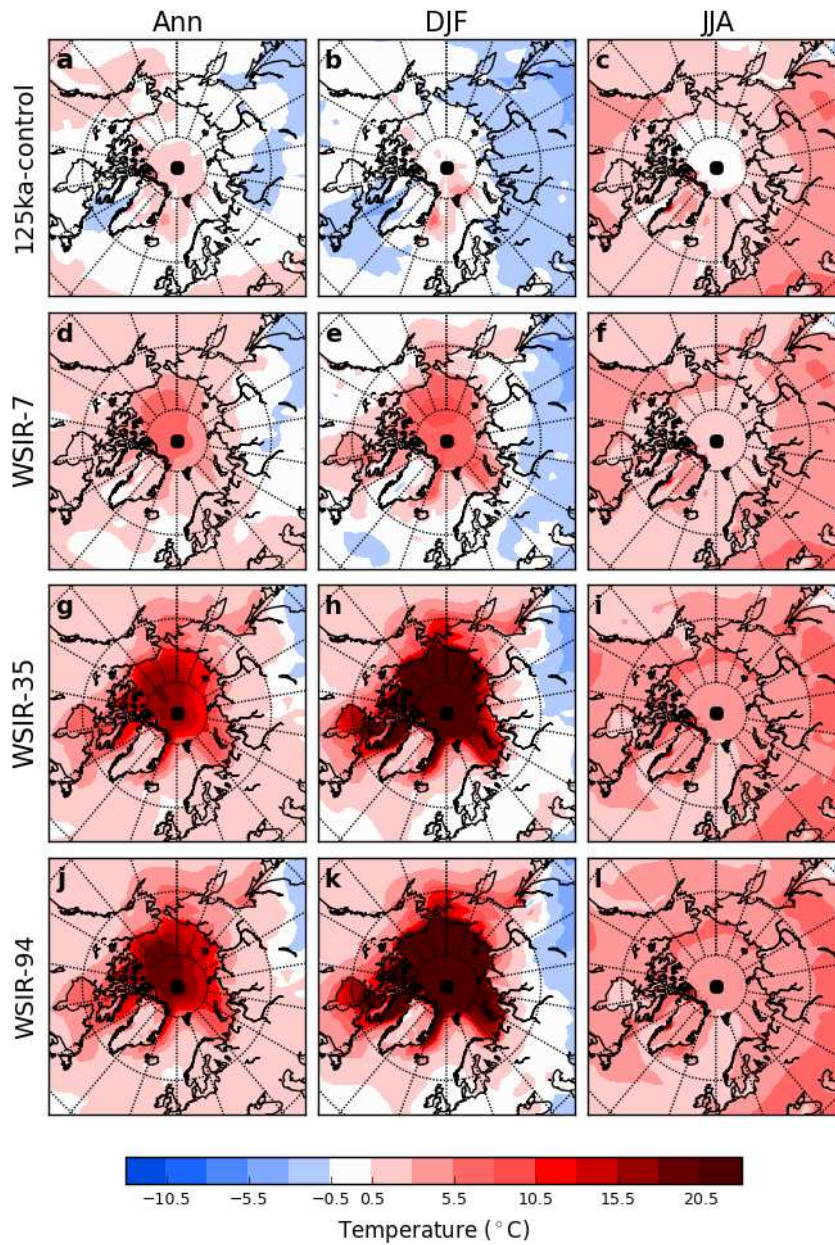
924

925

926

927

Figure 1. Change in the seasonal cycle of (a) temperature ($^{\circ}\text{C}$), (b) $\delta^{18}\text{O}$ (‰), and (c) precipitation (mm/month) at the NEEM deposition site. Anomalies are calculated between the 125 ka simulations using heat fluxes of 0 W m^{-2} (125ka-control, dark blue), 15 W m^{-2} (WSIR-7, green), 100 W m^{-2} (WSIR-35, red) and 200 W m^{-2} (WSIR-94, cyan) compared to the PI simulation. Also shown the annual cycle of Arctic sea ice extent (SIE – 10^6 km^2) in the LIG simulations.



928

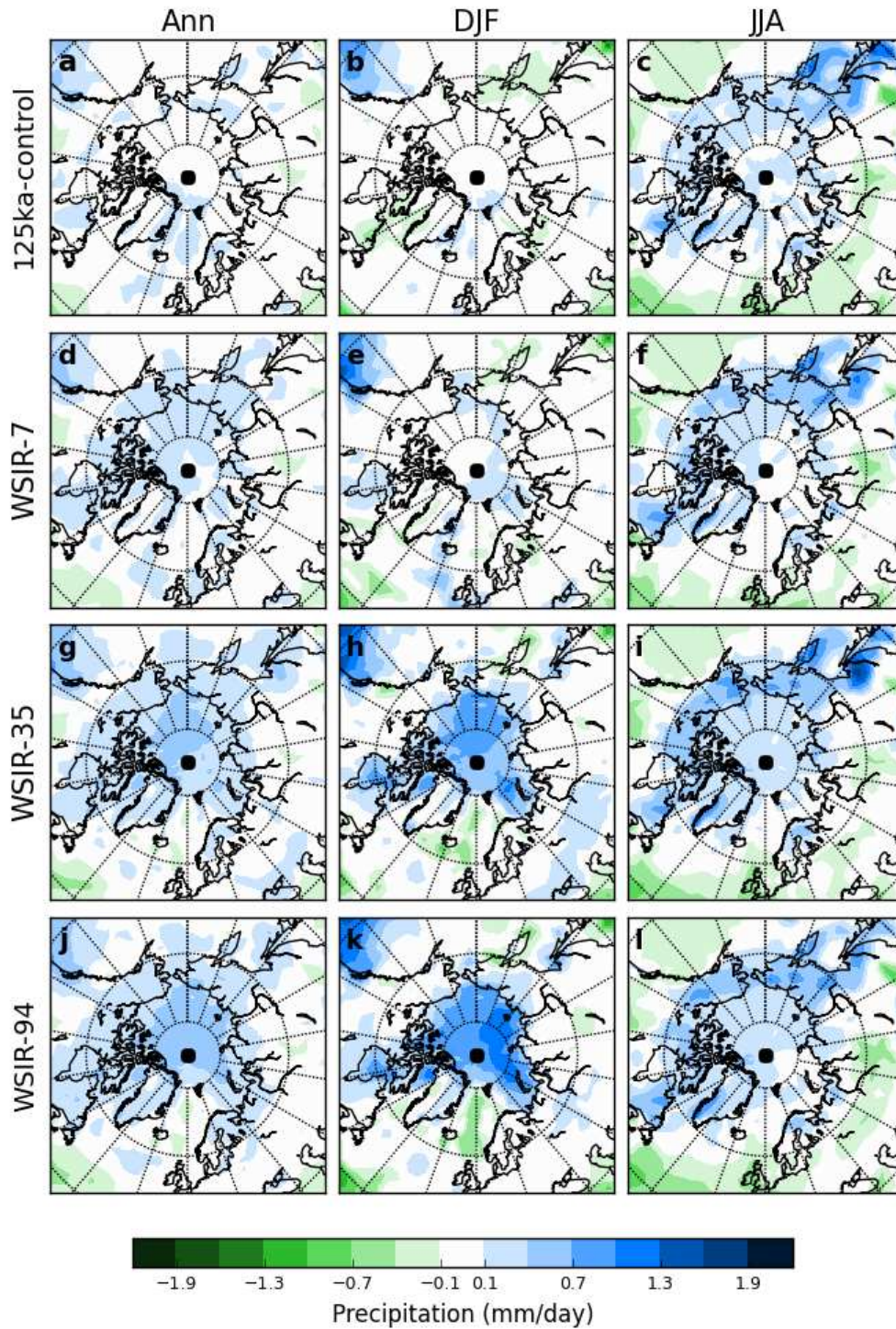
929

930

931

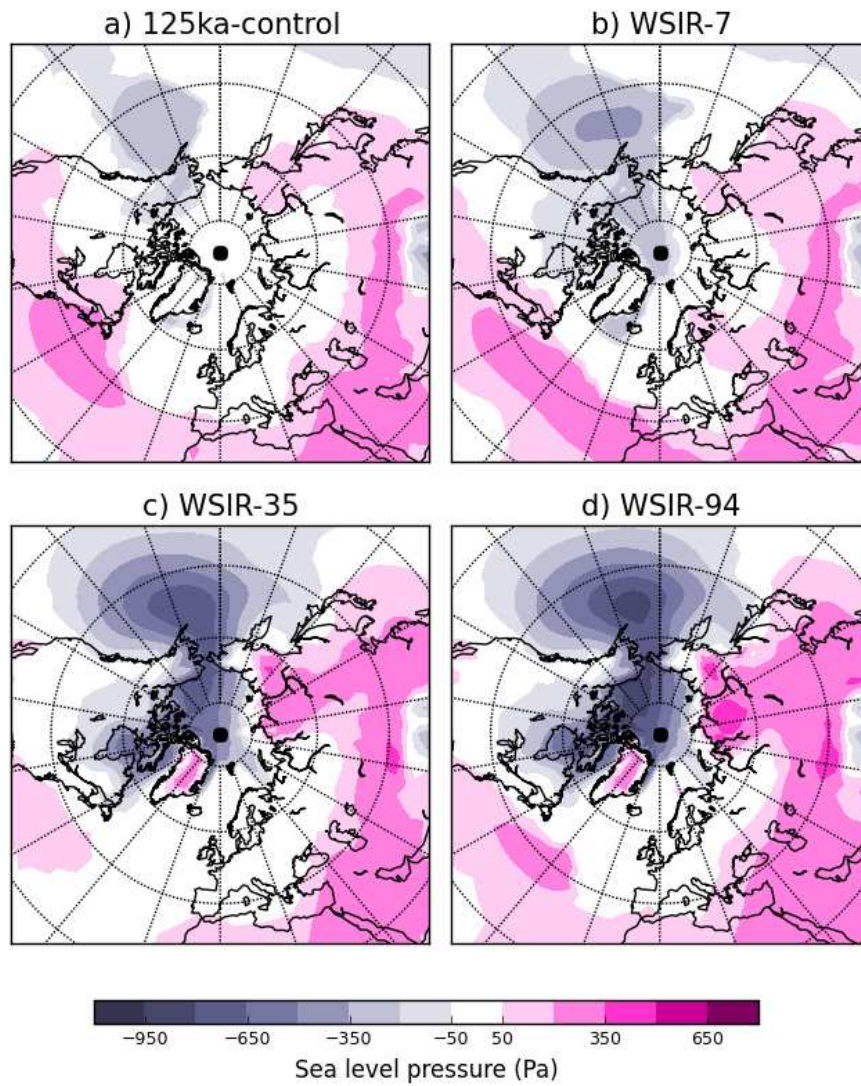
932

Figure 2. Modelled annual (ann), summer (JJA) and winter (DJF) surface air temperature anomalies for the 125ka-control simulation (a to c), WSIR-7 (d to f), WSIR-35 (g to i) and WSIR-94 (j to l) compared to the PI simulation. Only the anomalies statistically significant at the 95% confidence level are displayed.



933
 934
 935
 936
 937

Figure 3. Modelled annual (ann), summer (JJA) and winter (DJF) precipitation anomalies for the 125ka-control simulation (a to c), WSIR-7 (d to f), WSIR-35 (g to i) and WSIR-94 (j to l) compared to the PI simulation. Only the anomalies statistically significant at the 95% confidence level are displayed.



938

939

940

941

Figure 4. Modelled winter sea level pressure anomalies (Pa) for: a) 125ka-control, b) WSIR-7, c) WSIR-35 and d) WSIR-94 compared to the PI simulation. Only the anomalies statistically significant at the 95% confidence level are displayed.

942

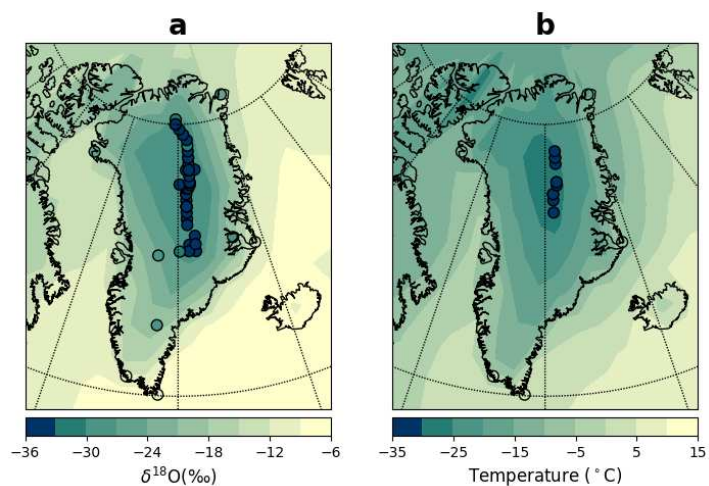
943 **Appendix A. Model evaluation**

944 In this section, we provide an evaluation of two control (PI and present-day experiments)
945 HadCM3 isotope simulations over Greenland. Previous work by Sime et al. (2013), using the
946 atmosphere only component of this model (HadAM3), has shown that annual Greenland means
947 of both isotopic values and surface temperatures are on average 8.6‰ too heavy and 1.9°C too
948 warm respectively, compared with present-day observations compiled by by Vinther et al.
949 (2010) and Sjolte et al. (2011). Following on from this, HadCM3 surface temperatures and
950 isotopic values are compared with the observational data provided by Vinther et al. (2010) and
951 Sjolte et al. (2011) (see Sime et al., 2013 for estimates and locations of individual records).

952 Comparison with observations indicates an annual warm bias over Greenland of 2.2°C for the
953 PI simulation and 3.7°C for the present-day simulation (figure A.1b). Note, most observational
954 sites are located in central Greenland, providing an unequal representation of the whole of
955 Greenland. Hence, the comparison can be considered more representative of the cold central
956 Greenland region (see figure A.1b for the position of the observational sites).

957 The $\delta^{18}\text{O}$ results follow a similar pattern (figure A.1a). Comparison with the observations
958 suggests that both the PI and present-day simulations are on average 5.8‰ and 7.1‰ (figure
959 A.1a) too heavy respectively. Some other models show similar heavy $\delta^{18}\text{O}$ biases (e.g.
960 Hoffmann et al., 1998; Sjolte et al., 2011; Sime et al., 2013). Sime et al. (2013) point to the
961 inaccurate seasonal representation of the isotopes in precipitation as a possible reason for the
962 model-data isotopic offset.

963 It would be expected that similar bias affect the PI and LIG simulations. Therefore, to reduce
964 the impact of model bias over Greenland, and hence any effects on the study results, we follow
965 the standard approach of reporting modelled values as anomalies (PI minus LIG).



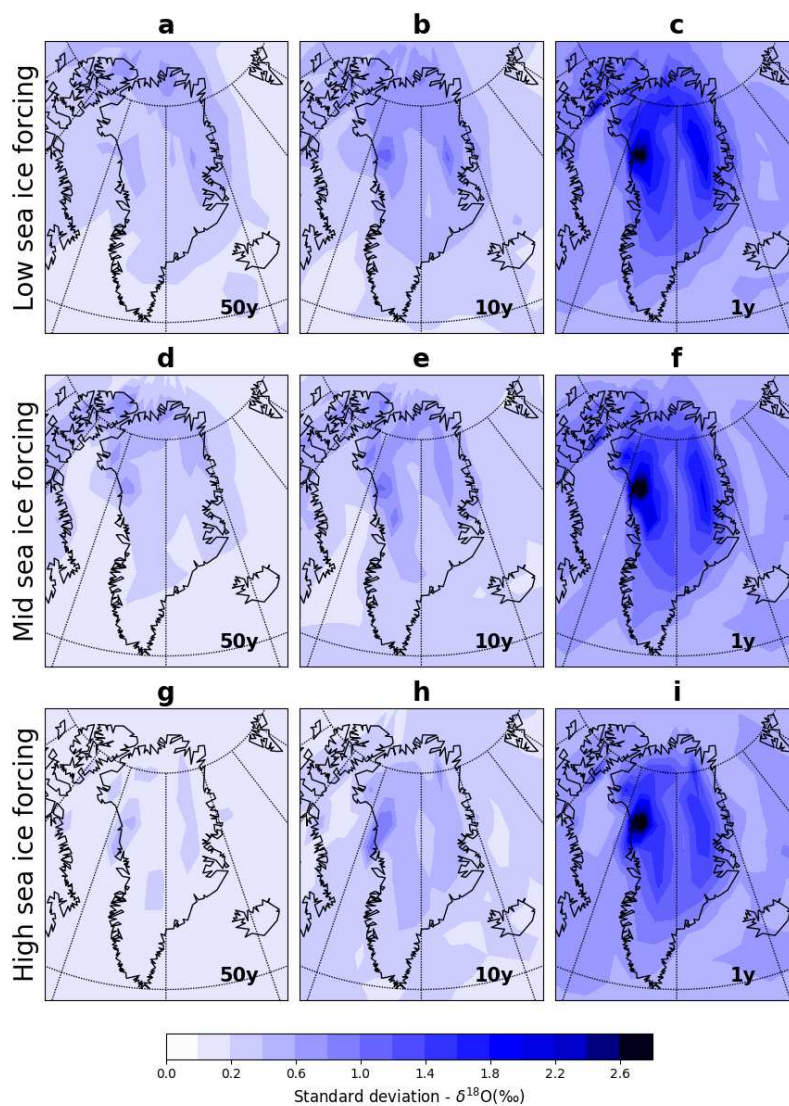
966

967
 968
 969
 970
 971
 972
 973

Figure A1. Present-day observations of $\delta^{18}\text{O}$ and temperature (Vinther et al., 2010; Sjolte et al., 2011) superimposed onto modelled present-day (1950-2000) values. (a) Annual $\delta^{18}\text{O}$ (‰) and (b) annual surface temperatures (°C). Seven transient present-day simulations covering the period 1850-2004 are considered for this analysis. In particular, the shading on each plot shows the mean of these seven present-day simulations for the period 1950-2000.

974 **Appendix B. Modelled uncertainty on $\delta^{18}\text{O}$**

975 Figure B.1 shows the simulated annual to decadal variability of annual mean $\delta^{18}\text{O}_p$ for a low,
976 medium and high sea ice forcing. $\delta^{18}\text{O}_p$ variability is larger near the coast at both annual and
977 decadal time scales (figure B.1). For the sea ice forcing ensemble, at all ice core sites, decadal
978 isotope variability (ranging from standard deviations of 0.36‰ up to 0.62‰ depending on the
979 site) is lower relative to the annual variability (ranging from standard deviations of 0.88‰ up
980 to 1.6‰ depending on the site) (table B.1).



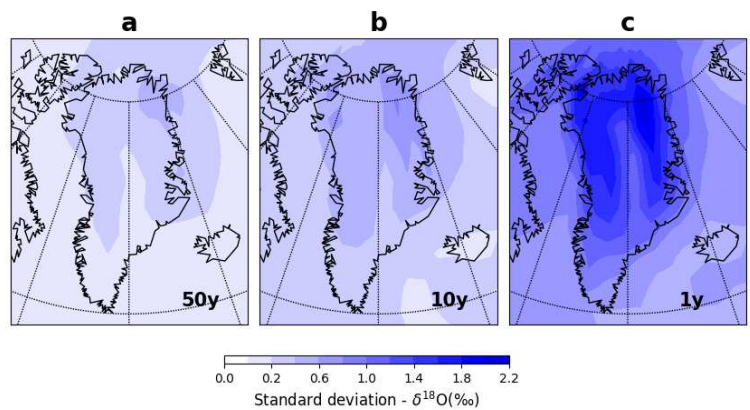
981

982 **Figure B1.** Variability of annual mean $\delta^{18}\text{O}_p$ for a low (a-c), medium (d-f)
983 and high (g-i) sea ice forcing, at 50-year average (a, d, g), decadal (b, e, h)
984 and annual (c, f, i) time scales. In particular, the shading in each plot shows
985 the standard deviation between sea ice retreat experiments with a low
986 (between 7% and 19%), medium (between 21% and 65%) and high
987 (between 72% and 100%) winter sea ice loss compared to the PI simulation.

988 **Table B1.** Modelled variability of annual mean $\delta^{18}\text{O}_p$ at seven ice cores sites at 50-year average, decadal
 989 and annual time scales. We list standard deviations (‰) for the sea ice retreat experiments ensemble and a
 990 present-day scenario. For the present-day scenario, the standard deviation between seven present-day
 991 experiments covering the period 1850-2000 is presented.

Ice core sites	Sea ice forcing ensemble			Present-day forcing scenario		
	Standard deviation (‰)			Standard deviation (‰)		
	50-year average	Decadal	Annual	50-year average	Decadal	Annual
NEEM	0.24	0.47	1.3	0.22	0.50	1.4
NGRIP	0.24	0.45	1.3	0.19	0.46	1.3
GRIP	0.23	0.36	1.0	0.15	0.34	1.0
Renland	0.28	0.45	1.1	0.33	0.51	1.3
Camp Century	0.35	0.62	1.6	0.30	0.65	1.7
DYE3	0.19	0.37	0.88	0.19	0.36	1.0
GISP2	0.23	0.37	1.1	0.17	0.36	1.1

992 To complement this model uncertainty analysis on annual mean $\delta^{18}\text{O}_p$ values, the standard
 993 deviation of 50-year averages are also estimated as this is the time-window used to report all
 994 isotope averages in this study. Figure B.1 shows the modelled variability of 50-year averages
 995 for a low, medium and high sea ice forcing. For the sea ice forcing ensemble, the standard
 996 deviation at this 50-year time scale does not exceed (1) 0.19‰ at DYE3, (2) 0.23‰ at GRIP
 997 and GISP2, (3) 0.24‰ at NEEM and NGRIP, (4) 0.28‰ at Renland and, (5) 0.35‰ at Camp
 998 Century (table B.1).



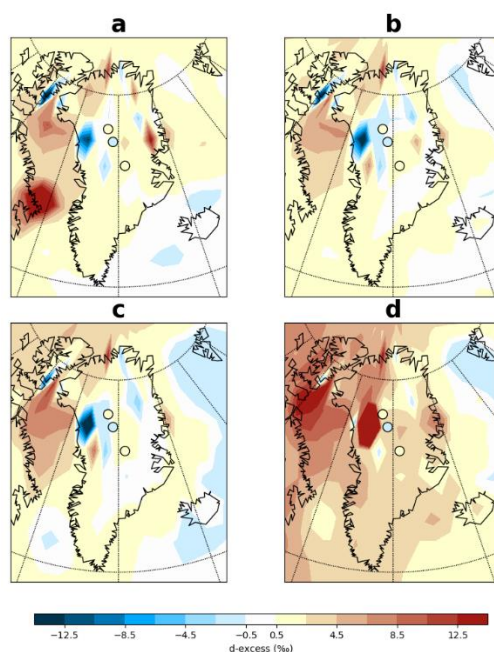
999
 1000 **Figure B2.** Variability of annual mean $\delta^{18}\text{O}_p$ for a present-day scenario at
 1001 (a) 50-year average, (b) decadal and (c) annual time scales. In particular,
 1002 the shading in each plot shows the standard deviation between seven
 1003 present-day experiments covering the period 1850-2000.

1004 For comparison, we also calculated the variability of annual mean $\delta^{18}\text{O}_p$ for a present-day
 1005 scenario at annual, decadal and 50-year average time scales (figure B.2). At all ice core sites,

1006 the simulated annual, decadal and 50-year average variability of $\delta^{18}\text{O}_p$ for the present-day
1007 forcing scenario is very similar relative to the sea ice forcing ensemble (table B.1).

1008 **Appendix C. Annual deuterium excess changes**

1009 Deuterium excess (hereafter d-excess) has been previously used as a proxy for source area
1010 conditions (e.g. Masson-Delmotte et al., 2005; Steffensen et al., 2008). Figure C.1 shows
1011 results from the selected 125 ka simulations compared with d-excess data compiled by Landais
1012 et al. (2016). We obtain similar values of RMSE for d-excess for the 125ka control simulation
1013 (1.1‰), WSIR-7 (1.0‰) and WSIR-35 (1.1‰). The experiment WSIR-7 has the lowest
1014 (“best”) RMSE (1.0‰), whereas the WSIR-94 experiment shows the highest RMSE (3.4‰).
1015 The modelled d-excess results should however be interpreted with caution. The representation
1016 of micro-scale cloud physics in HadCM3 does not have a discernible impact on first order $\delta^{18}\text{O}$
1017 or δD , but does permit for some tuning of the d-excess (e.g. Tindall et al., 2009; Schmidt et al.,
1018 2007; Werner et al., 2011). Better knowledge and improved model representation of micro-
1019 scale cloud physics could permit a more insightful analysis of the d-excess data (Landais et al.,
1020 2016).



1021

1022

1023

1024

1025

1026

Figure C1. The d-excess data compiled by Landais et al. (2016) superimposed onto modelled annual d-excess anomalies relative to the PI simulation for: (a) 125ka control (RMSE = 1.1‰), (b) WSIR-7 (RMSE = 1.0‰), (c) WSIR-35 (RMSE = 1.1‰) and (d) WSIR-94 (RMSE = 3.4‰).

